



## Advancing nanofluid numerical modelling: A novel Euler–Lagrange method with experimental validation

N. Vovk<sup>a</sup>, B. Kamenik<sup>a</sup>, E. Begum Elcioglu<sup>c</sup>, E. Özyurt<sup>c</sup>, Z.H. Karadeniz<sup>d</sup>, A. Turgut<sup>b</sup>, J. Ravnik<sup>a</sup>\*

<sup>a</sup> Faculty of Mechanical Engineering, University of Maribor, Smetanova 17, SI-2000, Maribor, Slovenia

<sup>b</sup> Department of Mechanical Engineering, Dokuz Eylül University, Izmir, Turkey

<sup>c</sup> Department of Mechanical Engineering, Eskişehir Technical University, Eskişehir, Turkey

<sup>d</sup> Department of Energy Systems Engineering, Izmir Institute of Technology, Izmir, Turkey

### ARTICLE INFO

#### Keywords:

Euler–Lagrange nanofluid modelling  
Numerical uncertainty assessment  
Natural convection loop simulation  
Nanoparticle concentration analysis  
Nanofluid heat transfer

### ABSTRACT

We present a novel approach to numerical modelling of thermal nanofluids based on the Euler–Lagrange method. This approach overcomes the challenge of extremely fine temporal discretization, which previous Euler–Lagrange nanofluid numerical models struggled to address, while also avoiding the need for too many Lagrangian nanoparticles. A numerical uncertainty assessment method is adapted for the proposed approach. The model is validated with a simple verification case and applied to simulate a closed natural circulation loop heat exchanger operating with heating power ranging from 10 W to 50 W and nanoparticle volume fractions of 0.5% to 2%, using an Al<sub>2</sub>O<sub>3</sub>–water nanofluid. Results are compared with experimental temperature measurements and an Euler–Euler implementation of the same nanofluid. The model is also applied to simulate the natural convection inside a vertical enclosure, studied experimentally by other authors. The proposed novel approach demonstrates agreement with both experimental data and the Euler–Euler implementation, effectively capturing the overall behaviour of nanofluids. We establish, that the interplay of multiple transport phenomena, that occur in nanofluid operated devices, can be difficult to completely reproduce numerically within the framework of current modelling assumptions.

### 1. Introduction

Passive heat exchangers are highly desirable solutions for systems where reliability is key. The disaster at the Fukushima–Daiichi nuclear power plant in 2011 was caused by the power failure of the auxiliary diesel generators. Their task was to cool the reactor core in an emergency. In the years following the disaster, many concepts for passive heat dissipation were developed for nuclear power plants. Among those, some of them are based on natural convection loops (NCLs) [1–3], which eliminate the need for pumps with an external power supply. In such applications, the choice of working fluid directly determines the performance of the device. To increase the efficiency of heat exchangers, thermal properties of the working fluid must therefore be adapted. Traditionally, the primary working fluids have been water and water-based solutions such as water–ethylene glycol. The idea of nanofluids is that thermal properties of the working fluid should be improved by dispersing particles with a size of 100 nm or less in the base fluid. The material of the particles should be chosen so

that its thermal conductivity is far greater than that of the base fluid, thereby improving the overall effective thermal conductivity of the nanofluid [4].

Numerical modelling approaches for nanofluids can generally be divided into three categories. The first is the single-phase approach, which assumes that the volume fraction of nanoparticles varies very little throughout the computational domain. The resulting thermophysical properties are therefore constant for the entire system or vary only spatially with temperature. Although it has been recognized that the single-phase approach adequately captures the integral quantities of the device to which it was applied [5,6], such models are still unable to provide crucial details about the volume fraction of the nanoparticles and the fields of thermophysical properties. As a result, this approach is unable to account for the physics governing the transport of nanoparticles and therefore cannot be used to fully understand the operation of nanofluid-based devices [7–9]. Abouali et al. [10] showed that

\* Corresponding author.

E-mail addresses: [nejc.vovk@um.si](mailto:nejc.vovk@um.si) (N. Vovk), [blaz.kamenik@um.si](mailto:blaz.kamenik@um.si) (B. Kamenik), [ebelcioglu@eskisehir.edu.tr](mailto:ebelcioglu@eskisehir.edu.tr) (E.B. Elcioglu), [eozyurt@eskisehir.edu.tr](mailto:eozyurt@eskisehir.edu.tr) (E. Özyurt), [haktankaradeniz@iyte.edu.tr](mailto:haktankaradeniz@iyte.edu.tr) (Z.H. Karadeniz), [alpaslan.turgut@deu.edu.tr](mailto:alpaslan.turgut@deu.edu.tr) (A. Turgut), [jure.ravnik@um.si](mailto:jure.ravnik@um.si) (J. Ravnik).

<https://doi.org/10.1016/j.ijheatmasstransfer.2025.127247>

Received 10 January 2025; Received in revised form 18 April 2025; Accepted 11 May 2025

Available online 3 June 2025

0017-9310/© 2025 The Authors. Published by Elsevier Ltd. This is an open access article under the CC BY-NC-ND license (<http://creativecommons.org/licenses/by-nc-nd/4.0/>).

integral quantities, such as the heat transfer coefficient, of nanofluid-based systems with natural convection can be well estimated using available correlations, making the single-phase nanofluid simulations redundant. The second approach is the so-called two-fluid or Euler–Euler approach, where we simulate the nanoparticles as a continuous field, which allows us to capture the transport phenomena within the nanofluid more accurately than the single-phase model [11]. An alternative approach to Euler–Euler is the so-called Euler–Lagrange approach, in which we simulate the fluid as a continuous (Eulerian) phase and the particles as points, whereby the shape of the particles is not resolved [12,13].

Traditionally, the translational dynamics of particles has been simulated by solving the Maxey–Riley equation, which acts by adding implicit or explicit contributions of individual particle forces and then used to calculate the particle velocity by solving the resulting ordinary differential equation (ODE) [14]. For particles in the submicron range, two force contributions become particularly important: the thermophoretic force, which is responsible for the migration of the particles in the direction of the negative temperature gradient in the base fluid, and the Brownian force, which can be interpreted as self-diffusion of the particle cloud [15].

He et al. [16] performed a numerical simulation of a nanofluid flowing through a heated straight pipe under laminar flow conditions applying the Euler–Lagrange approach and validated the obtained results with an experiment. They considered TiO<sub>2</sub>–water nanofluid and determined the conductivity and viscosity correlations by performing measurements. They found good agreement between the simulation and experimental results and concluded that the heat transfer coefficient is most influenced by the increased thermal conductivity of the nanofluid. Rashidi et al. [17] investigated external flows of nanofluids using the Euler–Lagrange approach and found that the effects of Brownian motion on the heat transfer coefficients were stronger than the effects of thermophoretic force. A similar problem was investigated by Maskaniyan et al. [18], where they studied particles of different sizes (30 nm–0.5 μm) and the resulting force contributions. They found that for particles of 30 nm and smaller, the contribution of the Brownian force becomes larger compared to the inertial forces. A numerical study of the Euler–Lagrange nanofluid flow in a pipe by Sharaf et al. [19] showed that the volume fraction of nanoparticles at the walls is highly non-uniform, further disproving the relevance of the single-phase assumption. They also concluded that Brownian and thermophoretic forces play an important role in the deposition of nanoparticles under laminar conditions. Similar results have also been reported by other researchers [20–23]. It was analysed in a review by Habeeb et al. [24] that the Euler–Lagrange approach was superior to the Euler–Euler approach in many cases.

The numerical modelling of nanofluids with the Euler–Lagrange approach encounters the following difficulties:

- The point-particle approach assumes that each particle in the computational domain is simulated individually. When simulating systems of particles of nanometre size, the number of Lagrangian particles can become very large even at small volume fractions of the dispersed phase, which greatly increases the computational costs. This problem is particularly pronounced when simulating real industrial devices, such as heat exchangers.
- The second obstacle when simulating nanofluids with the Euler–Lagrange approach is the computational time step size. We can calculate the response time of a Al<sub>2</sub>O<sub>3</sub> nanoparticle of size 25 nm suspended in water as follows

$$t_0 = \frac{\rho_p d_p^2}{18\mu_f} \quad (1)$$

and find that the response time is of the order of 10<sup>−10</sup> s. If one considers that the computational time step must be taken as a fraction of the particle response time [15], the problem of computational costs becomes even more pronounced.

The first problem is often addressed in the literature by considering a cluster of particles as a representative parcel, instead of simulating each nanoparticle individually. Rashidi et al. [17] simulated the parcels as a cluster of 5000 to 30 000 nanoparticles and computed the volume fraction in the finite volume cell as

$$\varphi_c = \frac{n_p^{\text{parcel}} V_p}{V_c}, \quad (2)$$

where  $V_c$  is the volume of the cell and  $n_p^{\text{parcel}}$ ,  $V_p$  are the number of nanoparticles in the parcel and the nanoparticle volume respectively. A similar approach was also adopted by other authors [25,26].

A more sophisticated approach was chosen by Mahdavi et al. [9, 27,28]. They computed the volume fraction of the nanoparticles by interpolating the Lagrangian field onto the Eulerian finite volume mesh using the Gaussian function centred on the particle centroid as

$$G_w = \left(\frac{a}{\pi}\right)^{3/2} \exp\left[-a \frac{|\vec{r}_{\text{parcel}} - \vec{r}_{\text{particle}}|^2}{\Delta x^2}\right], \quad (3)$$

where  $G_w$  is the Gaussian weight function,  $\vec{r}_{\text{parcel}}$  and  $\vec{r}_{\text{particle}}$  are the positions of the parcel and particle, and  $a$  is the Gaussian parameter that determines the influence of the volume fraction through the surrounding Eulerian finite volume mesh. The authors reported that the parameter  $a$  influences the volume fraction field and had little effect on the integral parameters, such as the heat transfer coefficient. The authors only chose  $a = 6$  as an appropriate value for their study, but acknowledged that further investigation was needed to determine the optimal value of  $a$  [9]. To the best of our knowledge, no in-depth research has been conducted on this topic to date.

Although progress has been made in solving the problem of the number of particles in the simulations, the problem of the small time step remains unsolved. This is mainly due to the state-of-the-art approach of Lagrangian particle tracking, which, as mentioned above, works by integrating the ODE that dictates the particle motion. This means that the application of an appropriate time step greatly increases computational costs [9,19].

For the numerical simulation to be accurate, both the numerical and modelling errors must be minimal. The former can be estimated using the well-known methods such as Richardson extrapolation, where we evaluate the discretization errors via the numerical uncertainty [29] and which is similar for all numerical methods, regardless of the physics involved. However, the modelling error depends on the physical properties of the working fluid and can be minimized by accurate experimental measurements. Unfortunately, there is still no standardized methodology for measuring the thermophysical properties of nanofluids [30]. Furthermore, the lack of consensus on reporting heat transfer coefficient makes it difficult for researchers to properly compare their results [30–32]. In this study, we use experimental measurements of the thermophysical properties of the nanofluid obtained through our own investigations, allowing us to obtain mathematical correlations of the thermophysical properties of the nanofluid as a function of temperature and volume fraction, to be used in simulations.

The main objective of this work is to implement a new method for modelling nanofluids using the modified Lagrangian approach, which addresses the above-mentioned difficulties of a high number of simulated nanoparticles and a small computational time step. The presented study offers several important contributions:

- Based on the physical assumption of a short response time of nanoparticles, the modified Lagrangian particle tracking method is implemented, which eliminates the need to solve the Maxey–Riley ODE.
- An approach similar to that of Mahdavi et al. [9,27,28], was considered for the calculation of the nanoparticle volume fraction field from the discrete field of Lagrangian particles. We use the so-called concentration blob method presented by Marshall and

Sala [33] and investigate the parameter for the radius of the concentration blob, which corresponds to the parameter  $a$  in Eq. (3), and determine its optimal value for simulations of nanofluid-based heat exchangers. In this context, Lagrangian particles are the actual computational particles in simulations, and nanoparticles are the physical particles, modelled using the proposed approach.

- The numerical model is verified using a simple verification case and compared with the solution obtained by solving the 1D volume fraction equation.
- We analyse the numerical uncertainty of the proposed numerical nanofluid model and introduce a method to quantify this uncertainty using a modified Richardson extrapolation technique.
- The experimental measurements are performed for the thermophysical properties of the  $\text{Al}_2\text{O}_3$ -water nanofluid. The obtained correlations are then used to test the performance of the numerical model on a NCL heat exchanger and validated against experimental temperature measurements as well as against the Euler-Euler implementation of the same nanofluid.

## 2. Experimental setup

### 2.1. The NCL heat exchanger

To validate the NCL heat exchanger simulation, measurements were carried out on a laboratory scale NCL heat exchanger, which is shown in Fig. 1. The NCL heat exchanger has a central heating element in the lower section with a length of 110 mm. At the top is a cooling section with a length of 140 mm, which ensures a constant temperature of 294 K. Copper pipes were selected for the experimental setup as they have excellent thermal conductivity and are easy to form. The outer diameter of the copper pipe is 6.63 mm with an inner diameter of 4.75 mm. The thermocouples are 96 mm away from the lower and upper pipe centreline.

Plastic pipes were installed on top of the NCL, which serve both as an expansion tank and as a simple fluid exchange point. A water jacket for the cooling area was 3D printed from ABS material and coated with epoxy to ensure it remains watertight. The thermocouples have a diameter of 1 mm, which could result in blockage of the flow area by 5% when inserted into the copper pipe. To minimize the effects of this blockage on the flow dynamics, the thermocouples were positioned in direct contact with the fluid, remaining close to the inner wall of the pipe. A nickel-chromium heating wire of appropriate length was wrapped around the intended heating area of the system to provide the necessary power. To prevent electrical contact between the heating wire and the electrically conductive copper pipe, a layer of insulating tape with high thermal conductivity was applied to the heating zone. An Aim-TTi CPX400DP programmable DC power supply was used to generate the heat input to the loop via the heater wire by controlling the supplied current and the voltage. The arrangement of the thermocouples for measuring the flow temperature is shown in Fig. 2.

Once all the thermocouples had been installed, the system was tested for leaks. It was operated for two hours with pure water at different heat outputs (10 W, 30 W and 50 W). The system was then allowed to cool down before being used again. This procedure confirmed the absence of leaks, even under the conditions of thermal expansion and contraction at different heater settings, thus confirming the integrity of the system.

The fabricated water jacket, shown in detail Y in Fig. 1, was coated with epoxy resin and subjected to a second round of leakage tests. After successful completion of these tests, the system was completely isolated. The experimental setup was then mounted on a frame made of aluminium profiles. The constructed NCL with all the piping prepared for the experiments is shown in Fig. 3.

### 2.2. Temperature measurements with the NCL operated by nanofluid

For the experimental setup, a cooled CLS CLRC-17 circulation bath was used, which can maintain a constant cooling water temperature with a sensitivity of 0.1 °C. A voltage and current controlled power supply provided steady power to the system via the heating wire throughout the experiments. Temperature measurements were recorded using K-type thermocouples, with data logging performed by an ORDEL UDL-100 Universal Data Logger. The setup also included thermocouples to monitor the inlet and outlet temperatures of the water jacket. A temperature validation study was conducted using deionized water at three different heating powers, with each experiment repeated twice over a three-day period to ensure consistency. The measurement uncertainty of the thermocouples is estimated to be  $\pm 0.5$  K.

## 3. Methods

The numerical calculations and post-processing were carried out using the open source software OpenFOAM, version 11 [34] and ParaView, version 5.12 [35]. A novel approach was integrated into the baseline solver for the coupling of liquid and nanoparticles. The NCL heat exchanger geometry consists of the nanofluid region and the copper pipe region. The multi-region approach was chosen to simulate the experiment more accurately by capturing the heat conduction from the heating region through the copper pipe.

### 3.1. Thermophysical properties of the $\text{Al}_2\text{O}_3$ -water nanofluid

In this study, we prepared the nanofluid samples using the two-step method. The nanoparticles used had an average diameter of 25 nm, as provided by the manufacturer. While we did not perform additional characterizations, we ensured proper dispersion through stirring (for sufficient amount of time and rotation), which provided the necessary stability during the thermophysical property measurements and heat transfer experiments. Absence of any stabilizing additives and ultrasonication was intentional, since these strongly affect the thermophysical properties and heat transfer performance, and our aim in this work was to keep the conditions of numerical analyses and experiments the same.

The dynamic viscosity and the thermal conductivity of the  $\text{Al}_2\text{O}_3$ -water nanofluid were measured in a temperature range from 20 °C to 60 °C and for three bulk nanoparticle volume fractions of 0.5%, 1% and 2%. The measurements were fitted using the least-squares method to obtain the mathematical correlations used in the simulations. Fig. 4 depicts temperature-nanofluid viscosity relation of the data of this work, along with the experimental data provided by Chandrasekar et al. [36] for 1% and 2%  $\text{Al}_2\text{O}_3$ -water nanofluids with 43 nm particle size, Mehta & Subhedar [37] for 0.5%  $\text{Al}_2\text{O}_3$ -water nanofluids with 20 nm particle size, Yiamsawas et al. [38] for 1% and 2%  $\text{Al}_2\text{O}_3$ -water nanofluids with 120 nm particle size, Elcioglu [39] for 1%, 2%, and 3% for  $\text{Al}_2\text{O}_3$ -water nanofluids with 10 nm and 30 nm particle size; together with the predictions of the Einstein model [40] ( $\mu = \mu_f(1 + 2.5\phi)$ ). Results showed that the measurements of this work are in good agreement with the data by Yiamsawas et al. [38], Mehta & Subhedar [37], and Elcioglu [39], following similar temperature-viscosity trends. Particle size-viscosity relation is not straightforward and there has been no consensus on particle size effect on nanofluids' viscosity. The reason for this is two-folded: (i) the sole effect of the particle size cannot be isolated from particle-particle interaction and cluster formation, and (ii) it is time- and process conditions-dependent and when and under what conditions viscosities of nanofluid specimen were measured are unknown for literature comparisons. Nevertheless, giving a broader range for particle size parameter as in Fig. 4, i.e., 10–120 nm, it is possible to assess discrepancies/agreements based on the particle size. It is seen that, data of Yiamsawas et al. [38] for 120 nm particle size of 2% nanofluid (largest particle, high concentration) as well as data of Elcioglu [39] for 30 nm particle size of 3% nanofluid (nearly

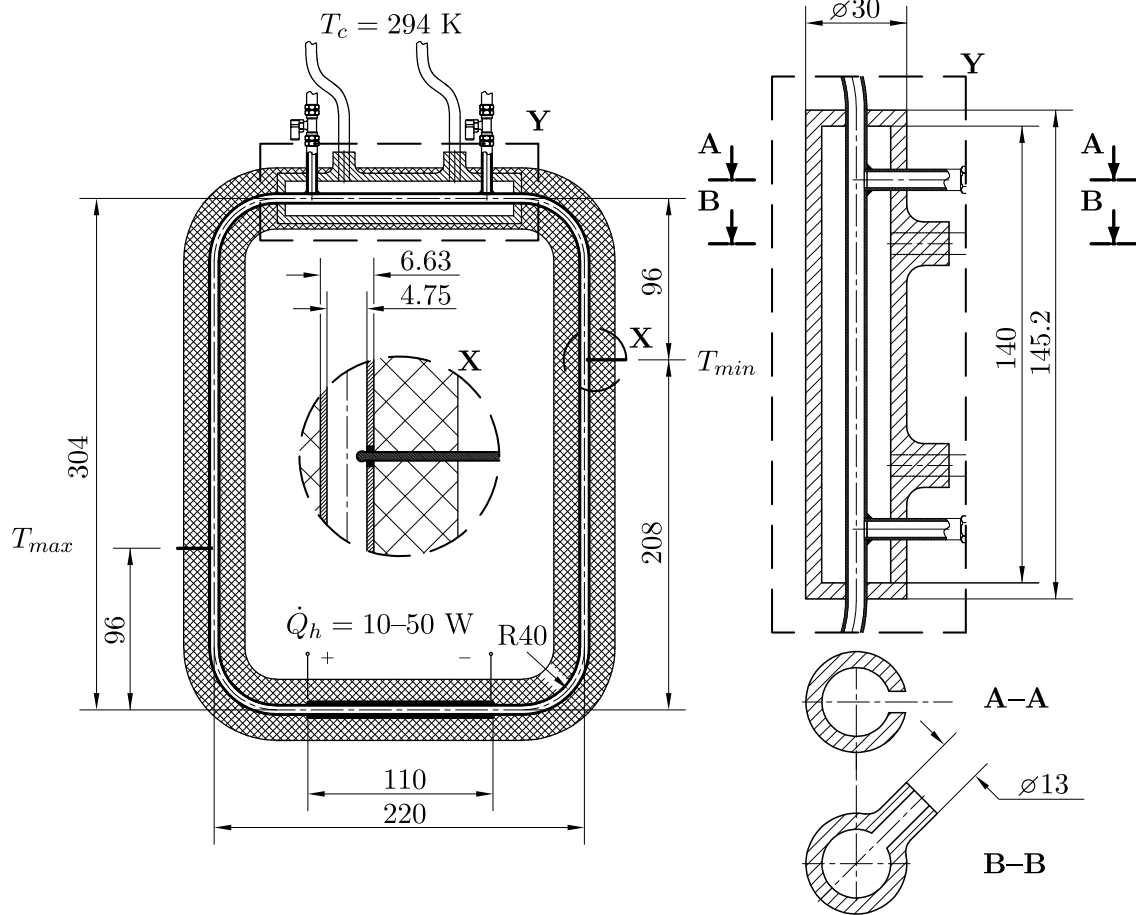


Fig. 1. Cross section of the nanofluid NCL heat exchanger geometry. The heating region is 110 mm long and the cooling region is 140 mm long. The subscripts *h* and *c* denote the heater and the cooler respectively.

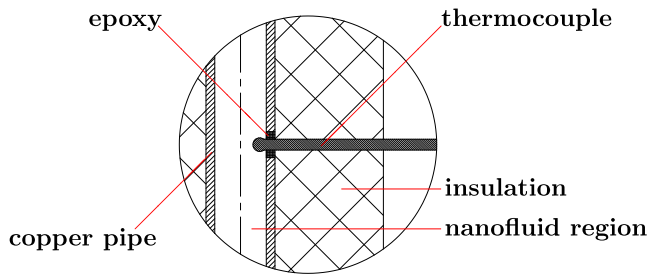


Fig. 2. Thermocouple installation detail.

equal size, concentration higher than studied) were extremes of the comparison dataset, and these data are higher than our measurements. All other measurements from the literature differ by an acceptable range from our measurements. It should be noted that the predictions of the Einstein model [40] were lower than our predictions, which is a widely observed trend in the literature.

Fig. 5 depicts temperature–nanofluid thermal conductivity relation of the data of this work, along with the experimental data provided by Turgut [41] for 1.5% Al<sub>2</sub>O<sub>3</sub>–water nanofluids with 25 nm particle size, Masuda et al. [42] for 1.3% Al<sub>2</sub>O<sub>3</sub>–water nanofluids with 13 nm particle size, Das et al. [43] for 1% Al<sub>2</sub>O<sub>3</sub>–water nanofluids with 38 nm particle size, Zhang et al. [44] for 1.2% Al<sub>2</sub>O<sub>3</sub>–water nanofluids with 38 nm particle size, and Murshed et al. [45] for 1% Al<sub>2</sub>O<sub>3</sub>–water nanofluids with 80 nm particle size; together with the predictions of the Maxwell model ( $k = k_f(k_p + 2k_f - 2(k_f - k_p)\phi)/(k_p + 2k_f + (k_f - k_p)\phi)$ ). Results

showed that the measurements of this work are in good agreement with the data by Turgut [41] at the studied temperatures and the data by Das et al. [43] at 20 °C. The data by Zhang et al. [44] have about 10% difference from our measurements. When a ±10% deviation range is considered, our data and the data by Zhang et al. [44], Turgut [41] and the predictions of the Maxwell model [46] appears in the same window. The data by Masuda et al. [42] and Murshed et al. [45] belong to extremes of the particle sizes in the comparison dataset, and that they have more than 10% difference from our data at studied temperatures. Here, the particle size–thermal conductivity relation being not monotonic can also be seen from Fig. 5.

The fitting was implemented by splitting the temperature and volume fraction dependencies into separate contributions. The following correlation was used for nanofluid viscosity:

$$\mu(T, \phi) = \sum_{i=0}^3 C_{\mu(T),i} T^i \cdot \sum_{j=0}^2 C_{\mu(\phi),j} \phi^j, \quad (4)$$

and for nanofluid thermal conductivity:

$$k(T, \phi) = \sum_{i=0}^3 C_{k(T),i} T^i \cdot \sum_{j=0}^2 C_{k(\phi),j} \phi^j. \quad (5)$$

The corresponding polynomial coefficients used are given in Table 1. The nanofluid density is estimated via the mixing rule:

$$\rho(T, \phi) = (1 - \phi) \sum_{i=0}^2 C_{\rho(T),i} T^i + \phi \rho_p. \quad (6)$$

The specific heat capacity of the Al<sub>2</sub>O<sub>3</sub>–water nanofluid at different bulk nanoparticle volume fractions are collected in Table 2. The

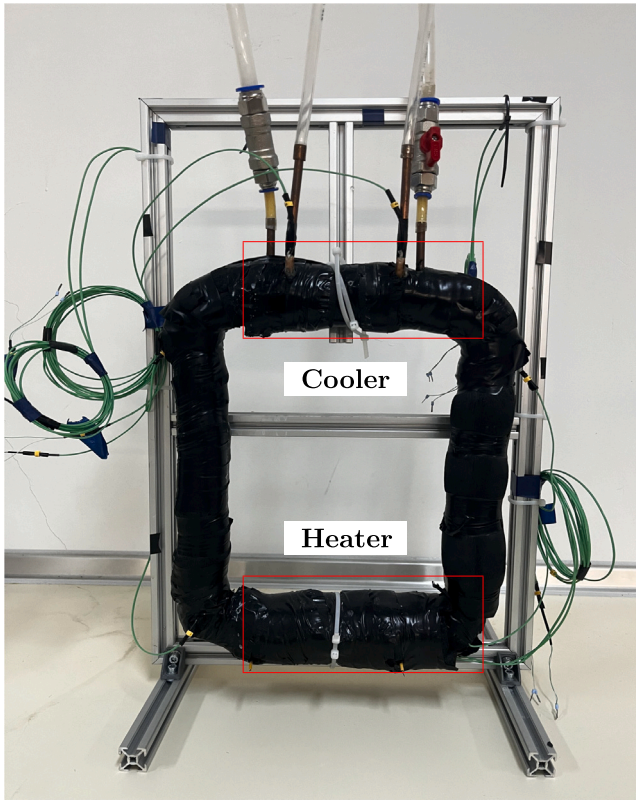


Fig. 3. The experimental NCL heat exchanger in realization.

Table 1

Polynomial coefficients for the  $\text{Al}_2\text{O}_3$ -water nanofluid thermophysical properties correlations in Eqs. (6)–(5). The presented polynomial coefficients correspond to the experimental measurements, presented in Figs. 4 and 5.

$i$	$C_{\rho(T),i}$	$C_{\mu(\varphi),i}$	$C_{\mu(T),i}$	$C_{k(T),i}$	$C_{k(\varphi),i}$
0	$8.213 \cdot 10^3$	$-7.523 \cdot 10^{-6}$	$9.644 \cdot 10^{-1}$	$9.128 \cdot 10^{-1}$	$4.882 \cdot 10^{-6}$
1	$1.482 \cdot 10^0$	$-1.852 \cdot 10^{-6}$	$-7.094 \cdot 10^0$	$2.062 \cdot 10^0$	$-6.017 \cdot 10^{-7}$
2	$-2.992 \cdot 10^{-3}$	$-7.092 \cdot 10^{-3}$	$3.760 \cdot 10^{-2}$	$3.015 \cdot 10^0$	$1.862 \cdot 10^{-4}$
3	0	0	$-5.054 \cdot 10^{-5}$	$-5.444 \cdot 10^{-3}$	0

Table 2

Specific heat capacity of the  $\text{Al}_2\text{O}_3$ -water nanofluid at different nanoparticle volume fractions, where  $\varphi_0$  denotes the bulk nanoparticle volume fraction.

Quantity	Symbol	Value
specific heat capacity at $\varphi_0 = 0.5\%$	$c_p^{0.5\%}$	4119.15 J/(kgK)
specific heat capacity at $\varphi_0 = 1\%$	$c_p^{1\%}$	4054.15 J/(kgK)
specific heat capacity at $\varphi_0 = 2\%$	$c_p^{2\%}$	3926.53 J/(kgK)

specific heat capacity was treated as a bulk property of the nanofluid and assumed constant over the entire temperature range for a given nanoparticle volume fraction. This assumption is supported by experimental measurements, which indicate minimal variation in specific heat capacity with temperature for the  $\text{Al}_2\text{O}_3$ -water nanofluid [5].

### 3.2. Eulerian method for the continuous phase

For fluid phase calculation, a system of Navier–Stokes equations for compressible laminar flow was used. The continuity and momentum equation are defined respectively as

$$\frac{\partial \rho}{\partial t} + \vec{\nabla} \cdot (\rho \vec{u}) = 0, \quad (7)$$

$$\frac{\partial (\rho \vec{u})}{\partial t} + \vec{\nabla} \cdot (\rho \vec{u} \vec{u}) = -\vec{\nabla} p^* - \vec{\nabla} \cdot \vec{\tau} + \rho \vec{g}, \quad (8)$$

where  $\rho$  is the density of the nanofluid, depending on the temperature and the volume fraction of the nanoparticles,  $\rho = \rho(T, \varphi)$ . The vectors  $\vec{u}$  and  $\vec{g}$  are the velocity and gravity. In the momentum equation (Eq. (8)), the corrected pressure  $p^*$  represents the absolute pressure with the hydrostatic component subtracted,  $p^* = p - \rho |\vec{g}| h$ . The term  $\vec{\nabla} \cdot \vec{\tau}$  represents the divergence of the stress tensor, where the latter is defined for compressible flows as

$$\vec{\tau} = 2\mu \bar{D} - \frac{2}{3}\mu (\vec{\nabla} \cdot \vec{u}) \bar{I}, \quad (9)$$

where  $\bar{D}$  is the strain rate tensor. In Eq. (9),  $\mu$  is the temperature and nanoparticle volume fraction dependent dynamic viscosity,  $\mu = \mu(T, \varphi)$  and  $\bar{I}$  represents the identity matrix. The energy equation is solved in the following form,

$$\begin{aligned} \frac{\partial (\rho h)}{\partial t} + \vec{\nabla} \cdot (\rho \vec{u} h) + \frac{\partial (\rho K)}{\partial t} + \vec{\nabla} \cdot (\rho \vec{u} K) \\ = \frac{\partial p^*}{\partial t} - \vec{\nabla} \cdot (k \vec{\nabla} T) + \rho_p c_p (D_B \vec{\nabla} \varphi + \vec{u}_T) \cdot \vec{\nabla} T + \rho (\vec{u} \cdot \vec{g}), \end{aligned} \quad (10)$$

where  $h$  is the enthalpy,  $K$  the kinetic energy, calculated as

$$K = \frac{1}{2} |\vec{u}|^2, \quad (11)$$

and  $k = k(T, \varphi)$  nanofluid thermal conductivity, dependent on temperature and nanoparticle volume fraction. The term  $\rho_p c_p (D_B \vec{\nabla} \varphi + \vec{u}_T) \cdot \vec{\nabla} T$  accounts for heat flux due to nanoparticle diffusion, as described by Buongiorno et al. [47]. The Brownian diffusivity,  $D_B$ , and the thermophoretic velocity,  $\vec{u}_T$ , are described in a later section. It must be emphasized that Eq. (10) solves for the enthalpy, where the Buongiorno heat flux, as well as the thermal diffusion term, are handled explicitly for the known temperature field from previous simulation time-step.

The heat conduction through the copper pipe is governed by the unsteady diffusion equation, as

$$\frac{\partial T}{\partial t} - \vec{\nabla} \cdot (k_{Cu} \vec{\nabla} T) = 0, \quad (12)$$

where  $k_{Cu}$  is the copper heat conduction coefficient.

#### 3.2.1. Boundary conditions for the finite volume method

The boundary conditions for the NCL heat exchanger are shown in Fig. 6. The temperature boundary conditions are Dirichlet type for the cooling surface of the copper pipe and Neumann type for the rest of the pipe outer surface. At the heating surface we prescribe the heat flux. To do this we set a fixed normal temperature gradient corresponding to the heating power used in the experiments with the thermal conductivity of copper set to  $k_{Cu} = 372 \text{ W/(mK)}$ . The boundary conditions for the wall between the fluid and the copper region were defined in such a way that the conservation of heat flow between the regions is fulfilled.

### 3.3. Lagrangian particle tracking

To track nanoparticles and estimate the location- and time-dependent volume fraction of nanoparticles in nanofluid, we propose the following approach. We assume that the nanoparticles in the flow field have a very low Stokes number. This means that the inertial forces are insignificant and the particles will follow the streamlines of the fluid. Li and Ahmadi [15] showed that very small particles ( $d_p < 0.05 \mu\text{m}$ ) are significantly dispersed by the Brownian force. It was also shown by Maskaniyan et al. [18] that this effect, together with the thermophoretic forces, cause the particles to diffuse across the streamlines. To express the above assumptions and build a numerical model for the motion of nanoparticles, we propose to track the particles by letting them follow the streamlines while their motion is perturbed by Brownian diffusion and thermophoresis at each time step:

$$\vec{r}_p^t = \vec{r}_p^{t-\Delta t} + \Delta \vec{r}_{p,B} + \Delta \vec{r}_{p,T} + \vec{u}_c \Delta t, \quad (13)$$

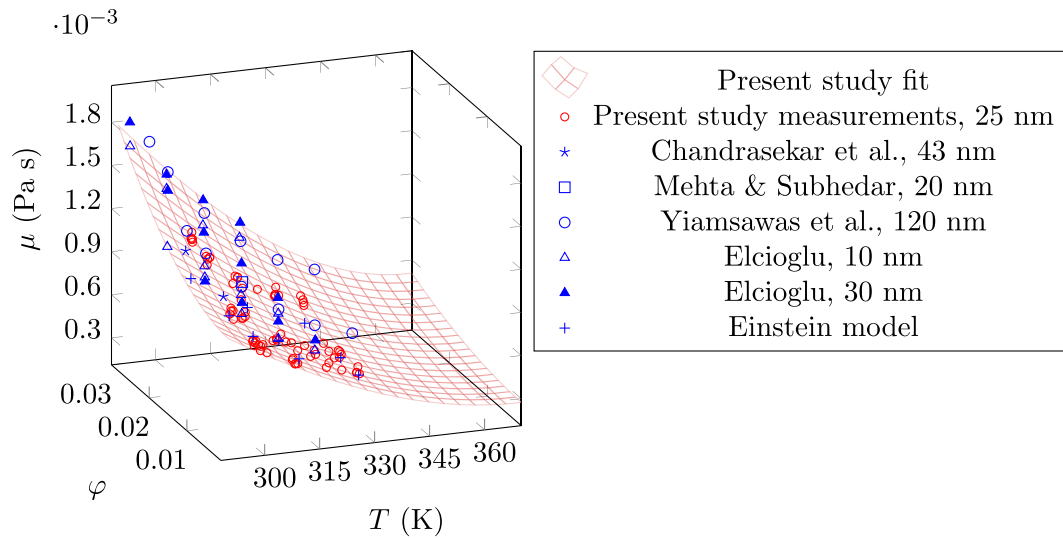


Fig. 4. Nanofluid viscosity relation of the data of this work, along with the experimental data provided by Chandrasekar et al. [36] for 1% and 2% Al<sub>2</sub>O<sub>3</sub>-water nanofluids with 43 nm particle size, Mehta & Subhedar [37] for 0.5% Al<sub>2</sub>O<sub>3</sub>-water nanofluids with 20 nm particle size, Yiamsawas et al. [38] for 1% and 2% Al<sub>2</sub>O<sub>3</sub>-water nanofluids with 120 nm particle size, Elcioglu [39] for 1%, 2%, and 3% for Al<sub>2</sub>O<sub>3</sub>-water nanofluids with 10 nm and 30 nm particle size; together with the predictions of the Einstein model [40] ( $\mu = \mu_f(1 + 2.5\phi)$ ).

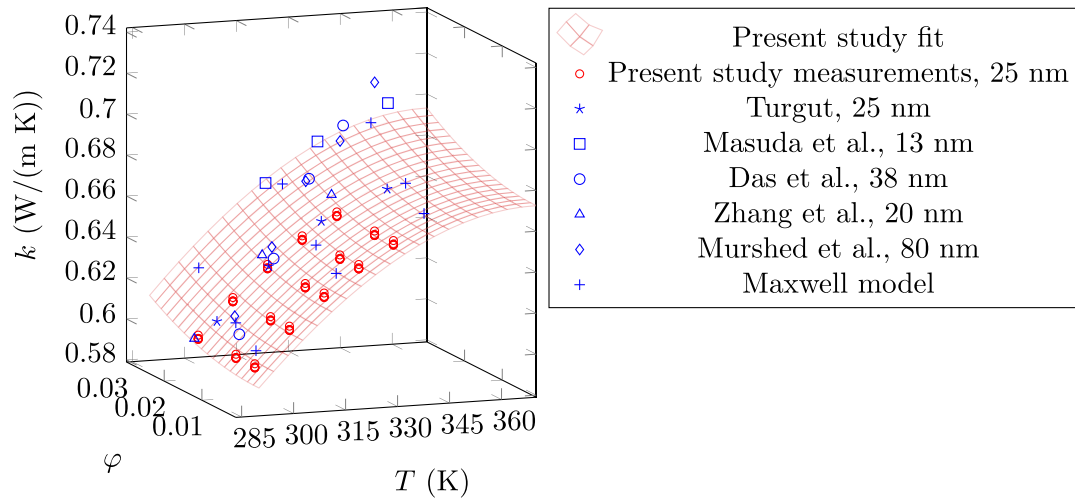


Fig. 5. Nanofluid thermal conductivity relation of the data of this work, along with the experimental data provided by Turgut [41] for 1.5% Al<sub>2</sub>O<sub>3</sub>-water nanofluids with 25 nm particle size, Masuda et al. [42] for 1.3% Al<sub>2</sub>O<sub>3</sub>-water nanofluids with 13 nm particle size, Das et al. [43] for 1% Al<sub>2</sub>O<sub>3</sub>-water nanofluids with 38 nm particle size, Zhang et al. [44] for 1.2% Al<sub>2</sub>O<sub>3</sub>-water nanofluids with 38 nm particle size, and Murshed et al. [45] for 1% Al<sub>2</sub>O<sub>3</sub>-water nanofluids with 80 nm particle size; together with the predictions of the Maxwell model ( $k = k_f(k_p + 2k_f - 2(k_f - k_p)\phi)/(k_p + 2k_f + (k_f - k_p)\phi)$ ).

where  $\vec{r}_p^t$  and  $\vec{r}_p^{t-\Delta t}$  denote the particle position vector at current and previous time step respectively,  $\vec{u}_c$  the fluid velocity at the Lagrangian particle position and  $\Delta t$  the simulation time step. Brownian motion is modelled as a random particle position perturbation,  $\Delta\vec{r}_{p,B}$ , calculated as [15]

$$\vec{r}_{p,B} = \vec{G}\sqrt{6D_B\Delta t}, \tag{14}$$

where  $D_B$  is the Brownian diffusivity, calculated as

$$D_B = C_c \frac{k_B T}{2\pi\mu_f d_p}. \tag{15}$$

In Brownian diffusivity definition,  $C_c$  is the Cunningham factor,  $k_B$  Boltzmann constant,  $T$  and  $\mu_f$  the temperature and the kinematic viscosity of the fluid and  $d_p$  the nanoparticle diameter. In modelling the stochastic nature of Brownian motion, we define a random vector  $\vec{G}$  as [15]:

$$\vec{G} = \vec{s}X, \tag{16}$$

where  $X$  is a normally distributed, zero mean, unit variance scalar, that dictates the magnitude of vector  $\vec{G}$ . The direction of  $\vec{G}$  is determined by the unit vector  $\vec{s}$ , which is defined as

$$\vec{s} = [\cos((u+1)\pi)\sqrt{1-b^2}, \sin((b+1)\pi)\sqrt{1-b^2}, b], \tag{17}$$

where  $b$  is a uniformly distributed random variable over the interval  $[-1, 1]$ . This formulation ensures that  $\vec{s}$  is a random unit vector, uniformly distributed over the surface of a sphere. The combination of  $\vec{s}$  and  $X$  means that  $\vec{G}$  is a random vector whose magnitude is normally distributed and whose direction is uniformly distributed on the unit sphere. To model the displacement due to Brownian motion, the vector  $\vec{G}$  is scaled by  $\sqrt{6D_B\Delta t}$ , meaning that the position perturbation magnitude will be normally distributed around  $\sqrt{6D_B\Delta t}$  and its direction will be uniformly distributed on a unit sphere, adequately capturing the random and isotropic nature of diffusion [15].

In Eq. (13),  $\Delta\vec{r}_{p,T}$  is the movement of the Lagrangian particle along the temperature gradient, because of thermophoresis, calculated

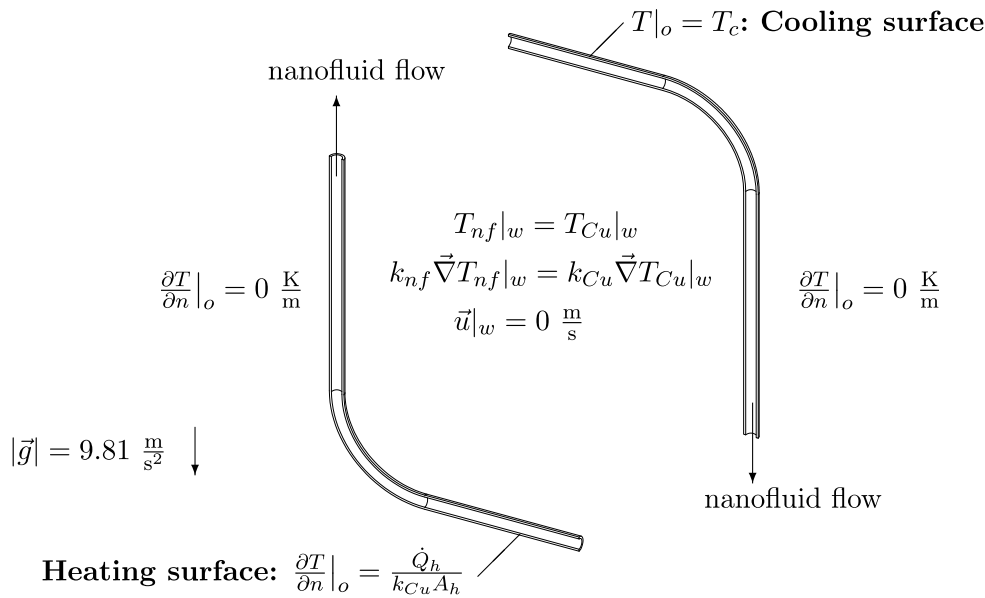


Fig. 6. Boundary conditions for the NCL heat exchanger multi-region simulation. Shown here, are the bottom left corner and the top right corner of the NCL. The subscript  $w$  denotes the inner surface of the copper pipe,  $o$  its outer surface,  $nf$  refers to the nanofluid region and  $Cu$  the copper pipe material.

as [47]:

$$\Delta \vec{r}_{p,T} = -\beta v_f \frac{\nabla T}{T} \Delta t, \quad (18)$$

where  $\beta$  is defined by the McNab–Meisen relation as [48]

$$\beta = 0.26 \frac{k_f}{2k_f + k_p}. \quad (19)$$

In a more recent study of the  $\text{Al}_2\text{O}_3$  nanoparticles by Aminfar & Haghgoo [49], the  $\beta$  coefficient was determined to be  $\beta(\varphi_0 = 0.01) = 0.018$  and  $\beta(\varphi_0 = 0.03) = 0.01$ . By linear interpolation of those values, we obtain the  $\beta$  coefficient for the bulk volume fractions, studied in this paper:

$$\beta^{0.5\%} = 0.02, \quad \beta^{1\%} = 0.018, \quad \beta^{2\%} = 0.014. \quad (20)$$

### 3.4. Nanoparticle volume fraction field calculation

In order to calculate new thermophysical properties of the nanofluid based on the local volume fraction of nanoparticles, the continuous volume fraction field,  $\varphi(\vec{r})$ , must be obtained from a discrete field of particles. In this context, the term Lagrangian particle refers to the computational particles used in the simulations, while nanoparticles represent the volume fraction distributions associated with these Lagrangian particles. The primary objective is to efficiently represent the volume fraction field of the nanoparticles with a minimum number of Lagrangian particles. We compute the volume fraction field as

$$\varphi(\vec{r}) = f \tilde{\varphi}(\vec{r}), \quad (21)$$

where parameter  $f$  ensures that the average nanoparticle volume fraction amounts to the bulk nanoparticle volume fraction, therefore satisfying the mass conservation. It is calculated as

$$f = \frac{V_0 \varphi_0}{\int_{V_0} \tilde{\varphi}(\vec{r}) dV}, \quad (22)$$

where  $V_0$  is the volume of the computational domain and  $\varphi_0$  the average nanoparticle volume fraction. The nanoparticle volume fraction at position,  $\tilde{\varphi}(\vec{r})$ , was computed from the Lagrangian particle positions using the concentration blob method [33],

$$\tilde{\varphi}(\vec{r}) = \sum_{p=1}^{n_p} \frac{2}{3\pi R_b^3} \exp\left[-\frac{|\vec{r} - \vec{r}_p|^2}{R_b^2}\right]. \quad (23)$$

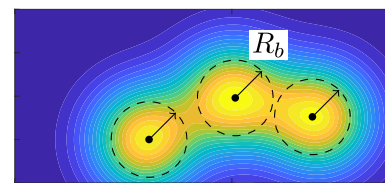


Fig. 7. Illustration of the concentration blob method. The black dots represent the Lagrangian particles, while the dashed circles represent the distance to the concentration blob radius, showing the influence of the nanoparticle volume fraction field around the Lagrangian particles.

The idea behind it is that one Lagrangian particle represents multiple physical nanoparticles in the system. The parameter  $R_b$  is the so-called concentration blob radius and tells how far away from the Lagrangian particle at position  $\vec{r}_p$  does the volume fraction influence reach. The concentration blob method essentially describes a Gaussian distribution of volume fraction around the given Lagrangian particle. To calculate the nanoparticle volume fraction field on the finite volume mesh, we set  $\vec{r}$  in Eq. (21) to the centre of each finite volume cell. The concentration blob method is illustrated in Fig. 7. The black dots represent the Lagrangian particles, while the dashed circles represent the distance to the concentration blob radius.

A better visualization of the influence of the radius of the concentration blob on the nanoparticle volume fraction field is shown in Fig. 8, where a simple finite volume block mesh is shown. Inside the finite volume mesh, a smaller bounding box is defined, where the Lagrangian particles are randomly distributed. The values of the concentration blob radius are reported in form of the relative concentration blob radius,  $R_b/\delta$ , where  $\delta$  is the average size of the finite volume cell in the domain. It can be seen that the volume fraction field is more spatially averaged with increasing size of the concentration blob radius. If we increase the radius of the concentration blob extremely, the proposed Euler–Lagrange method converges to the behaviour of the single-phase approach described in Section 1. By using the single-phase approach, we lose crucial insights into the volume fraction field and its influence on the fields of thermophysical properties.

### 3.5. Solution algorithm

The following algorithm is used to perform the simulation:

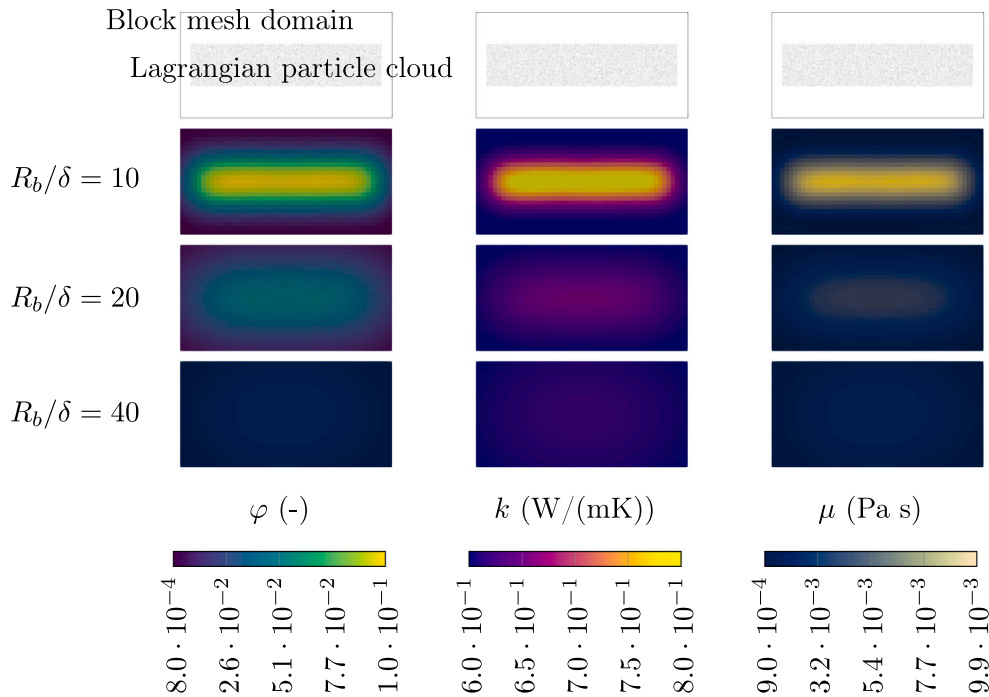


Fig. 8. Comparison of different  $R_b/\delta$  values and their influence on the instantaneous nanoparticle volume fraction field and the thermophysical properties for three cases. The bulk nanoparticle volume fraction is  $\varphi_0 = 0.02$ .

- Initially distribute Lagrangian particle randomly,
- initialize the nanoparticle volume fraction field, Eqs. (21)–(23),
- initialize the velocity, temperature and pressure fields with a constant value.
- Proceed with time loop:
  1. Compute dynamic viscosity and density fields, Eqs. (4), (6),
  2. solve Eq. (8) to obtain the velocity field,
  3. compute thermal conductivity field, Eq. (5),
  4. solve Eq. (12) to obtain the temperature field inside the copper pipe region,
  5. solve Eq. (10) to obtain the enthalpy field and perform the enthalpy — temperature conversion, to obtain the temperature field,
  6. preform PIMPLE pressure corrections to obtain the pressure field,
  7. evolve the Lagrangian particle cloud using Eqs. (13)–(19),
  8. compute the new nanoparticle volume fraction field, Eqs. (21)–(23),
- stop the simulation when quasi steady-state has been achieved.

## 4. Results

### 4.1. Verification of the nanofluid numerical model

To test the proposed Euler–Lagrange approach, we have developed a simple numerical 1D benchmark experiment to observe the temporal evolution of the nanoparticle volume fraction. We assume that the fluid does not move and is subjected to a constant temperature gradient. In such a case, when using the Euler–Euler approach, the transport equation for nanoparticle volume fraction can be written as follows:

$$\frac{d\varphi}{dt} = \frac{d}{dx} \left( D_B \frac{d\varphi}{dx} + D_T \frac{dT}{dx} \frac{1}{T} \right), \quad x \in [0, L], \quad t \in [0, \tau] \quad (24)$$

with zero flux boundary condition at both sides:

$$D_B \frac{d\varphi}{dx} \Big|_{x=0, x=L} + D_T \frac{dT}{dx} \frac{1}{T} \Big|_{x=0, x=L} = 0. \quad (25)$$

An in-house finite volume solver based on this Euler–Euler approach was prepared to compare the results with the newly proposed Euler–Lagrange approach. The volume fraction profiles were compared at  $\tau = 1000$  s. The computational domain has a length of  $L = 2.5$  mm. The fluid inside is stationary and is subject to a constant temperature gradient of  $dT/dx = 16\,000$  K/m in  $x \in [0, L]$ . The temperature at  $x = 0$  m was set to  $T_0 = 303$  K, so the temperature at  $x = L$  must be  $T_L = 343$  K to satisfy the temperature gradient. At  $\tau = 0$ , the nanoparticle volume fraction field was initialized to  $\varphi_0 = 0.03$  in the whole domain. The kinematic viscosity of the base fluid was set to  $\nu_f = 10^{-6}$  m<sup>2</sup>/s, the thermal conductivity of the fluid to  $k_f = 0.6$  W/(mK), the thermal conductivity of the nanoparticles to  $k_p = 25.0$  W/(mK) and the diameter of the nanoparticles to  $d_p = 20$  nm. For thermophoresis modelling, the McNab–Meisen [48] relation was used (Eq. (19)).

The concentration blob method (21)–(23) estimates the volume fraction field using two parameters: the radius of the concentration blob,  $R_b$  and the number of Lagrangian particles,  $n_p$ . To investigate their influence on the accuracy of the results, we analyse them in a non-dimensional way. We describe the influence of the concentration blob in terms of the relative radius of the concentration blob,  $R_b/\delta$ , where  $\delta$  is the cell length of the finite volume in our 1D validation case. In 2D and 3D, this becomes  $\delta = \sqrt{\Delta x \Delta y}$  and  $\delta = \sqrt[3]{\Delta x \Delta y \Delta z}$  respectively. The proposed non-dimensionalization allows us to determine the number of finite volume cells that are influenced by the concentration blob. To generalize the number of Lagrangian particles, we divide it by the number of finite volumes used in the discretization of the Eulerian part,  $n_p/n_c$ , where  $n_c$  is the number of finite volumes.

To test the performance of the novel approach, several  $R_b/\delta - n_p/n_c$  configurations were tested. We monitored the discrepancy between the Euler–Euler FVM approach and the present results of the Euler–Lagrange model by introducing the relative error:

$$e = \sqrt{\frac{\sum_{c=1}^{n_c} (\varphi(\vec{r}_c) - \varphi_{c,FVM})^2}{\sum_{c=1}^{n_c} \varphi_{c,FVM}^2}}, \quad (26)$$

where  $\varphi_{c,FVM}$  is the nanoparticle volume fraction in cell  $c$ , computed by the FVM and  $\varphi(\vec{r}_c)$  the volume fraction, computed by the proposed Euler–Lagrange approach in the same cell.

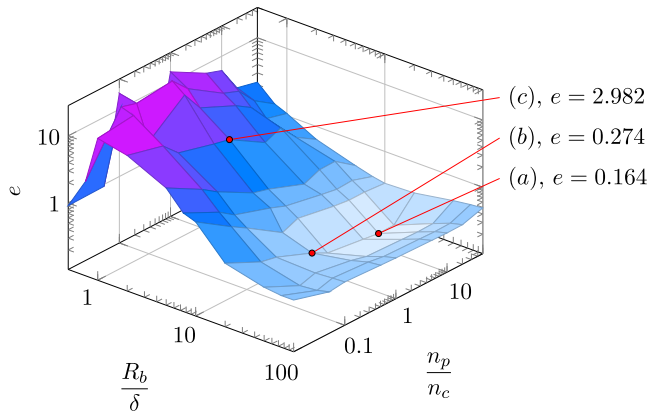


**Fig. 9.** The relative error phase diagram for different  $R_b/\delta$  and  $n_p/n_c$  configurations. The labels correspond to: (a)  $\rightarrow R_b/\delta = 20, n_p/n_c = 10$ ; (b)  $\rightarrow R_b/\delta = 20, n_p/n_c = 0.5$ ; (c)  $\rightarrow R_b/\delta = 2, n_p/n_c = 1$ .

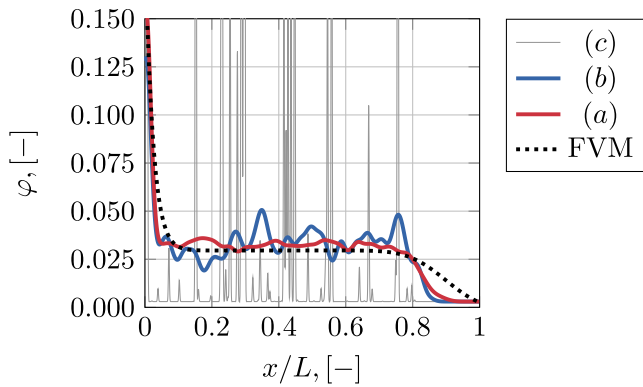


**Fig. 10.** Volume fraction profiles at  $\tau = 1000$  s compared between the FVM solution and our Lagrangian model. The (a), (b) and (c) lines correspond to blob radiuses and particle numbers shown in Fig. 9.

The relative error phase diagram is shown in Fig. 9 for  $0.1 \leq R_b/\delta \leq 100$  and  $0.5 \leq n_p/n_c \leq 100$ . The optimal configuration is seen in point (a), where  $R_b/\delta = 20, n_p/n_c = 10$ . The best fit of the volume fraction profiles is achieved when our computational domain contains 10 Lagrangian particles for every finite volume cell, and when the concentration blob spans over 20 cells.

Fig. 10 shows the comparison of three volume fraction profiles from the relative error phase diagram. The labels (a), (b) and (c) correspond to the points shown in Fig. 9. A big discrepancy from FVM results is visible in profile (c). This is due to the insufficient size of the concentration blob radius, thus, according to Eq. (23), the volume fraction values at the Lagrangian particle position are extreme.

In order to assess the numerical uncertainty of the considered approach, a Richardson extrapolation based method is proposed by modifying the algorithm shown by Celik et al. [29]. Richardson extrapolation is based on the representative discretization parameter,  $h$ . We define it as the ratio between the number of cells and the number of Lagrangian particles:

$$h = \frac{n_c}{n_p}, \quad (27)$$

so that as the number of Lagrangian particles tends to infinity, the  $h$  and the numerical error tend to zero. To estimate the convergence of the approach, we considered three consecutive cases with  $h = 10^{-4}, 10^{-1}, 0.25$  and correspondingly  $R_b/\delta = 1, 20, 20$ . We have chosen  $R_b/\delta = 1$  for  $h = 10^{-4}$  because with a high number of Lagrangian particles, which

**Table 3**  
Results of the modified GCI analysis for the verification case.

Parameter	Symbol	Value
Mean order of convergence	$\bar{p}$	0.159
Mean numerical uncertainty	GCI	5.5%

is of a similar order of magnitude as the number of nanoparticles, the concentration blob should not exceed a single finite volume cell. For the cases  $h = 10^{-1}, 0.25$  we chose  $R_b/\delta = 20$  based on Eq. (26). The extrapolation was conducted for volume fraction values in each finite volume cell separately. The extrapolated profile with the error bars is shown in Fig. 11, together with the most accurate solution  $h = 10^{-4}$ . Oscillatory convergence is observed in 50% of cells. The order of convergence ranges between  $p = 0.004-0.794$  with the mean value of  $\bar{p} = 0.159$ , which indicates poor convergence properties of the considered method. The mesh convergence index (grid convergence index, GCI [29]) ranges from GCI = 0.03% to 25.8% with the mean value of GCI = 5.5% and can be interpreted as a measure of numerical uncertainty. The reported high values are observed in  $x \in [0.85L, 0.95L]$ , therefore the maximum volume fraction uncertainty in that region accounts to approximately  $\pm 0.008$ . The numerical uncertainty assessment results are summarized in Table 3.

Fig. 12 shows the discrepancy between proposed Euler–Lagrange method results and the FVM results for two separate segments of the computational domain  $x/L \in [0.5, 1]$  in  $x/L \in [0.5, 1]$ . The purpose of plotting the relative error in separate segments is to see the error in regions with higher and lower nanoparticle volume fraction gradients. In the case of the point (a), the relative error in the first segment is lower than in the second segment, which can also be seen by looking at the segments in Fig. 10. This also shows that the relative error depends on the local number of Lagrangian particles as a result of thermophoresis. The second segment therefore contains a locally lower value of  $n_p/n_c$ , which explains the larger discrepancy, despite sufficient global  $n_p/n_c$ . The opposite effect can be observed in the first segment. There, a higher  $n_p/n_c$  is caused by thermophoresis and the agreement between the volume fraction profiles is therefore better.

The verification results obtained gave a good insight into the appropriate numerical parameters and the limitations of our model. When we use the model to simulate nanofluid heat exchangers, we need to consider the following:

- The number of Lagrangian particles in the heat exchanger computational domain must be 1–10 times the number of finite volume cells.
- The finite volume mesh must be constructed in such a way that we can define the radius of the concentration blob,  $R_b$ , so that it covers the volume in a radius of 20 cells around the Lagrangian particle.

#### 4.2. The NCL heat exchanger operated with water

In order to obtain a suitable finite volume mesh for the Eulerian part of the simulation, we simulated the NCL operated with water. Since there are no particles in water, we can focus exclusively on the discretization error of the Eulerian part. We consider three finite volume mesh designs. The numerical uncertainty values given are obtained using the method proposed by Celik et al. [29] and reported as the GCI for the fine and coarse finite volume mesh. Fig. 13 shows the structured hexahedral finite volume mesh with different number of cells used for the mesh independence analysis. The time step was selected as  $\Delta t = 0.01$  s and kept the same for all three mesh cases. The selected time step corresponds to the Courant number  $Co \approx 1$  for the finest mesh. We use the PIMPLE algorithm used in OpenFOAM to simulate pseudotransient problems. For each physical time step, we perform 5 PIMPLE iterations to obtain a convergent solution at each time step.

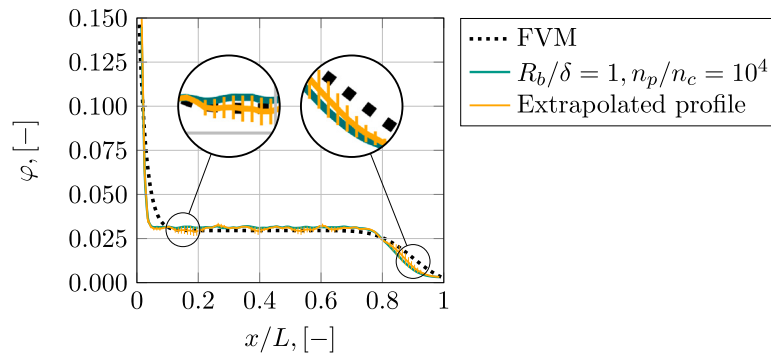


Fig. 11. The extrapolated profile with corresponding error bars and the  $h_1$  volume fraction profile. The mean order of convergence is  $\bar{p} = 0.159$  and the mean numerical uncertainty is  $GCI = 5.5\%$ .

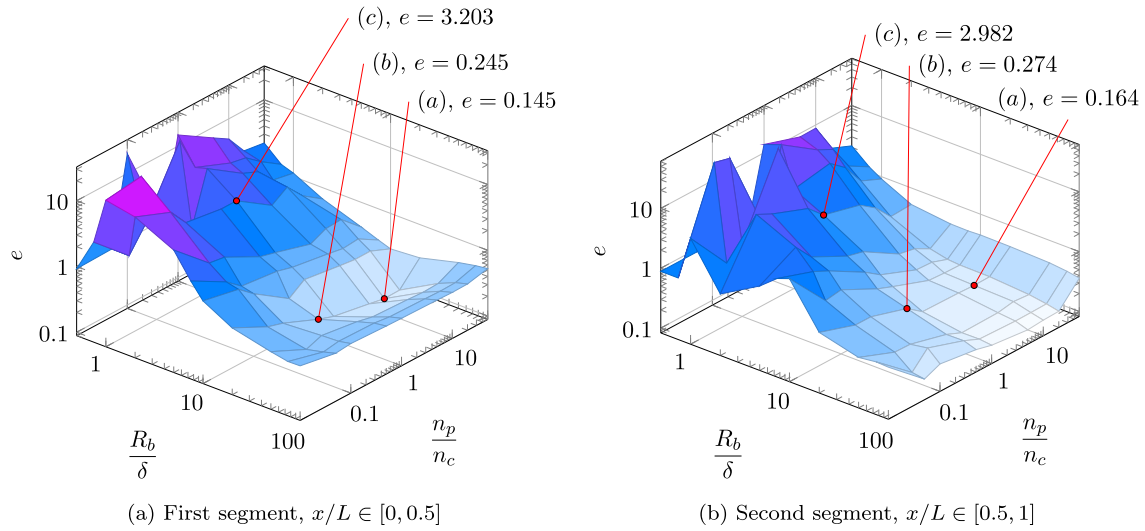


Fig. 12. Divided relative error phase diagram, for different  $R_b/\delta$  and  $n_p/n_c$  configurations. The phase diagrams are divided to show the relative error in two separate segments  $x/L$  of the verification computational domain. The labels (a), (b) and (c) correspond to the points, described in Fig. 9.

The numerical schemes employed are first order accurate for both the temporal and spatial discretization of the governing equations. This choice was motivated by the observation that higher order schemes could not accurately simulate laminar buoyant flow, leading to unphysical oscillations and poor results. In contrast, the first-order scheme provided physically meaningful and consistent results, as shown in the mesh convergence study. Although first-order schemes are known to introduce higher numerical diffusion, they were considered suitable for this study due to their robustness and ability to accurately capture the behaviour of laminar buoyant flow.

The reported solution variable was considered to be the temperature difference,  $\Delta T = T_{max} - T_{min}$ , marked on Fig. 1. The representative mesh spacing parameter  $h$  was taken to be

$$h = \frac{1}{n_c} \sum_{i=1}^{n_c} (V_{c,i})^{1/3}, \quad (28)$$

where  $V_{c,i}$  is the volume of the  $i$ -th finite volume cell. GCI calculation input parameters for multi-region NCL simulation operating with pure water are shown in Table 4.

The results of the GCI analysis can be found in Table 5 and indicate that the solution is well converged. The calculated convergence order is  $p = 1.406$ , which means a convergence rate between first and second order. The extrapolated results of the coarse and fine meshes are 19.931 K and 20.024 K respectively, their relative deviation is 0.47%, which is smaller than the uncertainty of the coarse mesh, which is 1.52%. Since the deviation between the extrapolated results of the coarse and fine mesh is within the uncertainty limits of the coarse mesh,

Table 4

GCI calculation input parameters for multi-region NCL simulation operating with pure water.

Parameter	Symbol	Value
$\Delta T$ at $h_1$	$\Delta T_{h_1}$	20.082 K
$\Delta T$ at $h_2$	$\Delta T_{h_2}$	20.177 K
$\Delta T$ at $h_3$	$\Delta T_{h_3}$	20.345 K
Mesh spacing for $3.942 \cdot 10^6$ cell mesh	$h_1$	0.1988 mm
Mesh spacing for $0.493 \cdot 10^6$ cell mesh	$h_2$	0.3976 mm
Mesh spacing for $0.162 \cdot 10^6$ cell mesh	$h_3$	0.5758 mm

we can safely use the coarse mesh for subsequent simulations without significant loss of accuracy.

#### 4.3. The NCL heat exchanger operated with nanofluid

In this section, we present the results of using the proposed Euler-Lagrange method to simulate the  $Al_2O_3$ -water nanofluid flow and heat transfer in the NCL heat exchanger. For the Eulerian part, we use the coarse mesh that we selected in Section 4.2. Based on the findings reported in Section 4.1 for the Lagrangian part, we use  $R_b/\delta = 20$  and  $n_p/n_c = 1$ , which gives approximately 161 000 simulated Lagrangian particles. For thermophoresis modelling, the Aminfar & Haghgoo [49] relation was used (Eq. (20)).

The result comparison for  $Al_2O_3$ -water nanofluid is presented in Fig. 14. The abbreviations Exp, EE, EL and SP denote the experiment,

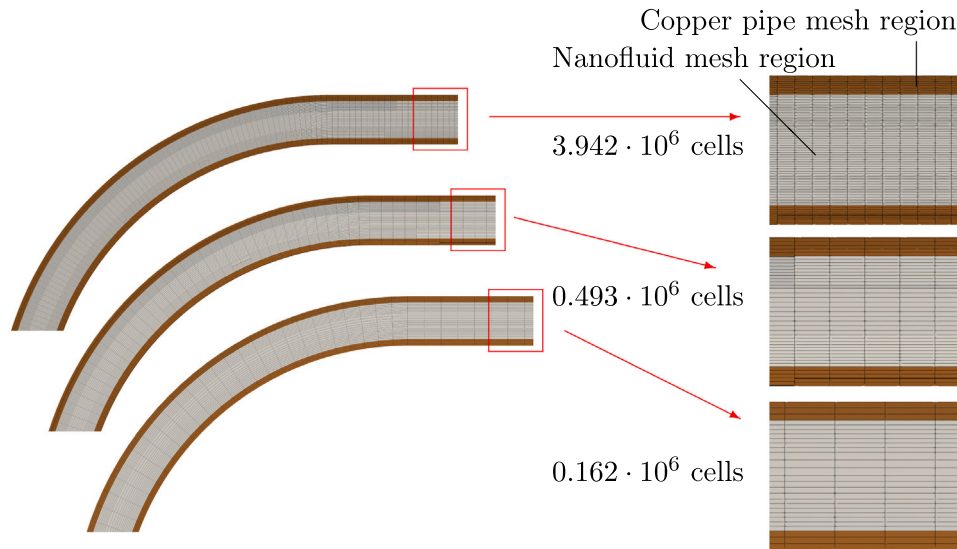


Fig. 13. Finite volume mesh, used for mesh independence analysis with pure water. The figure shows one of the elbows on the NCL.

Table 5  
Results of GCI analysis for multi-region NCL simulation operating with pure water.

Parameter	Symbol	Value
Order of convergence	$p$	1.406
Coarse mesh extrapolated result	$\Delta T_{\text{ext},32}$	19.931 K
Fine mesh extrapolated result	$\Delta T_{\text{ext},21}$	20.024 K
Coarse mesh numerical uncertainty	$GCI_{\text{coarse},32}$	1.52%
Fine mesh numerical uncertainty	$GCI_{\text{fine},21}$	0.36%

Euler–Euler [50], single-phase [50] and the present Euler–Lagrange implementations respectively. The reported uncertainty of experimental data for  $\Delta T$  is 1 K, which is indicated by the error bars in the plot. We observe, that all presented results follow the same trend. The EE, EL and SP results slightly underpredict the experimentally measured  $\Delta T$  result, while the EL approach, presented in this study, shows the best accuracy.

Fig. 15 plots the  $T_{\text{max}}$  (see Fig. 1) value versus the bulk nanoparticle volume fraction. A good agreement of the EL results is observed with the EE and the SP results, while an underprediction is observed, when comparing with the experimental results. The underprediction is constant and amounts to 4 °C–5 °C for the whole bulk nanoparticle volume fraction range as well as the heater power range. The EE, SP and the novel EL approach exhibit a consistent underprediction. This is reasonable, as all models rely on the same mathematical correlations presented in Section 3.1. The consistent underprediction is likely attributed to the definition of the boundary conditions. Although the heat exchanger was modelled as a multi-region domain, including both the nanofluid and copper pipe regions, certain effects were not accounted for. For instance, an adiabatic boundary condition was applied to the outer vertical walls of the pipe, whereas, in reality, heat loss occurs through this surface. Additionally, maintaining a strictly fixed temperature boundary condition on the cooler surface is experimentally challenging. Interestingly, the SP approach exhibits the same level of accuracy as the EE approach. Nonetheless, the EE and the present EL approaches are superior as they inherently capture the spatial non-homogeneity of the nanoparticle distribution, whereas this information is lost in the SP approach. It must also be emphasized, that the values of the specific heat capacities were taken constant for the whole temperature range, and only vary with the bulk nanoparticle volume fraction, which could affect the absolute temperature rise as an effect of the supplied heat in the computational domain.

Fig. 16 shows the temperature distribution in the NCL, which is operated with nanofluid, in a quasi-steady state. The fluid is heated

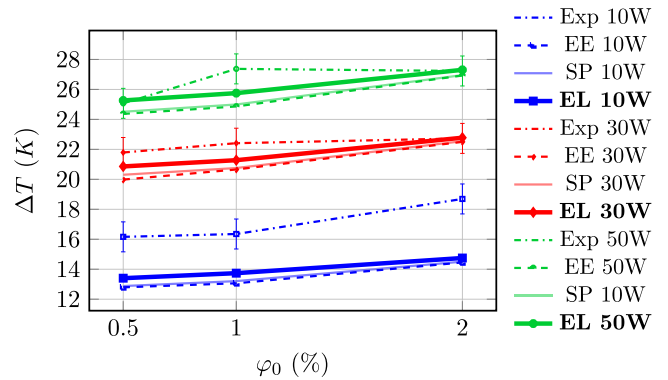


Fig. 14. The  $\text{Al}_2\text{O}_3$ –water nanofluid NCL heat exchanger results for  $\Delta T = T_{\text{max}} - T_{\text{min}}$ . The abbreviations Exp, EE, SP and EL denote the experiment, Euler–Euler [50], single-phase [50] and the present Euler–Lagrange results respectively.

with a constant heat flux at the bottom and cooled with a constant temperature at the top, as specified in the definition of the boundary conditions in Section 3.2.1. Achieving the quasi-steady conditions is a computationally lengthy process, as the fluid in the NCL is initially stationary. The heat flow supplied at the bottom of the NCL heats the fluid symmetrically around the vertical axis, creating two fluid circulation areas that start at the bottom centre and expand symmetrically to the left and right. Only when the conditions become too unstable, i.e. when the density gradient that drives natural convection becomes too great, does the fluid rotate clockwise or counterclockwise. The choice of direction of fluid rotation is therefore determined by the minimum numerical inaccuracy of the solver’s calculation of the density gradient and was found to be completely random. If we use the McNab–Meisen [48] relation for modelling thermophoresis, the  $T_{\text{max}}$  becomes slightly lower;  $\sim 1.4\%$  at the highest bulk volume fraction and heater power.

Fig. 17 shows the volume fraction of the nanoparticles in the NCL. The values are normalized to the bulk volume fraction, so that better comparison of the volume fraction fields could be made between all cases. The fields shown here are time-averaged over the period of 500 s to 700 s, which amount to 15–30 passages of the particles around the NCL, depending on the average flow rate of the nanofluid in the NCL, which is mostly dictated by the supplied heat flux. The stopping times of the simulations were chosen at a point, where the temperature and

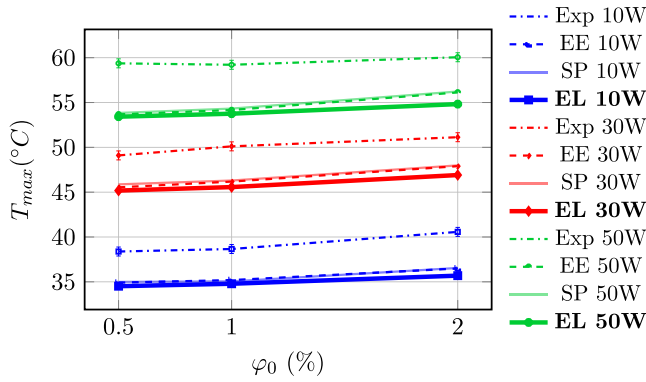


Fig. 15. The  $\text{Al}_2\text{O}_3$ -water nanofluid NCL heat exchanger results for  $T_{max}$ . The abbreviations Exp, EE, SP and EL denote the experiment, Euler-Euler [50], single-phase [50] and the present Euler-Lagrange results respectively.

the volume fraction fields reached quasi steady-state. Their values were monitored on the run via probes inside the computational domain, as well as the residual values, that reached orders of  $10^{-6}$  for the enthalpy and  $10^{-5}$  for the velocity components.

In the streamwise direction the transport of nanoparticles is convection dominated. That means, that the Brownian diffusion as well as thermophoresis have very little effect in the streamwise direction. This observation is particularly evident for the latter case, as the temperature gradients in the wall-normal direction are significantly larger—by orders of magnitude—than those in the streamwise direction, as observed from Fig. 16.

#### 4.4. Natural convection inside a vertical square enclosure

To further demonstrate the versatility of the proposed approach, we present the results of the present nanofluid numerical model, compared with the natural convection inside a vertical square enclosure experiment, conducted by Ho et al. [51]. The geometry of interest consists of a simple box enclosure with dimensions  $25 \text{ mm} \times 25 \text{ mm} \times 60 \text{ mm}$ . The enclosure is filled with the  $\text{Al}_2\text{O}_3$ -water nanofluid and is heated with constant heat flux on one side, and cooled with constant temperature on the other side, as schematically shown in Fig. 18. The heat flux on the hot wall is provided by an electric foil heater, while the cold wall includes internal channels, where the cooling fluid circulates and is regulated by the circulation water bath. The whole enclosure is insulated with 40 mm styrofoam. The authors report a mean diameter of the nanoparticles of 33 nm, although they later report that, during operation, the mean diameter increases with higher volume fraction to a mean of 148 nm. The details about the experimental apparatus can be found in the Ref. [51]. The numerical settings were the same as with the NCL, i.e.  $R_b/\delta = 20$  and  $n_p/n_c = 1$ . A mesh study of 37 000, 150 000 and 300 000 cells was made with pure water, from which we chose to use 150 000 cell, structured hexahedral mesh for the nanofluid simulations. The time-step was chosen, so that it corresponds to  $Co = 0.1 \sim 0.2$  for all simulations.

The results of the present nanofluid numerical model were compared to the experiment for the bulk nanoparticle volume fraction range of 1% to 3%. The hot wall heat flux range was  $|\vec{q}_h| = 273\text{--}2892 \text{ W/m}^2$  and the cold wall temperature was set to  $T_c = 295.15 \text{ K}$ , while the remaining walls were assumed to be adiabatic. In order to compare the numerical and experimental results, the surface-averaged heat transfer coefficient was evaluated in the quasi-steady state as [51]:

$$\overline{H} = \frac{|\vec{q}_h|}{\overline{T}_h - T_c}, \quad (29)$$

where  $\overline{T}_h$  is the surface-averaged temperature on the hot wall.

The results are shown in Fig. 19. The authors of the experiment report a mean experimental uncertainty of 15% for the surface averaged heat transfer coefficient, as indicated by the error bars on the figure. We observe the same trend in our model results as in the experiment, although a slight underprediction is observed. An inconsistency is observed in the experimental results, where, for example, the measured heat transfer coefficient ratio decreases from the 2 K to the 4 K temperature difference. This behaviour deviates from the expected trend, which generally indicates an increase in the heat transfer coefficient ratio with increasing temperature difference. Such anomalies cannot be captured by the numerical model, which is based on idealized physical assumptions that typically predict monotonic relationships — i.e., if one parameter increases, the corresponding response is also expected to increase. These discrepancies highlight the influence of complex or unaccounted — for phenomena in the nanofluid behaviour, that are not reflected in the current numerical framework.

As previously discussed by the authors of the experiment [51], at lower temperature differences, diffusive transport mechanisms play a more dominant role. In contrast, at higher temperature differences, convective effects become increasingly significant, not only for heat transfer but also for the transport of nanoparticles. This shift in dominant transport mechanism tends to suppress the distinct nanoparticle-related phenomena observed at lower temperature gradients. The observed minimal difference in heat transfer enhancement between the 33 nm and 148 nm nanoparticle simulations suggests that the relative influence of nanoparticle diameter is small. In our model, the particle diameter determines the magnitude of the Brownian force, which is of the same order of magnitude than the thermophoretic contribution. However, both contributions are much smaller than the drag, and thus the resulting nanoparticle distribution in the domain is most heavily influenced by the velocity field of the fluid. As a result thermophysical properties, which depend on nanoparticle concentration, are not greatly influenced by particle diameter.

## 5. Conclusions

In this study, a modified Euler-Lagrange approach for the simulation of nanofluids was developed, implemented and tested. The accuracy and capabilities of the method were thoroughly evaluated. The developed method was used to simulate performance of a real natural convection loop (NCL) heat exchanger operated by a nanofluid, as well as the natural convection inside a vertical enclosure. We used a  $\text{Al}_2\text{O}_3$ -water nanofluid and measured its thermophysical properties in a temperature range of  $20 \text{ }^\circ\text{C}$  to  $60 \text{ }^\circ\text{C}$  and the bulk nanoparticle volume fraction range of 0.5% to 2%. The measured values were used to obtain mathematical correlations for temperature and nanoparticle volume fraction dependent thermophysical properties, which were used in subsequent NCL and vertical enclosure simulations.

The following summarizes the main conclusions:

- The concentration blob method for estimating the nanoparticle volume fraction field on the Eulerian finite volume mesh using the particle positions uses two parameters: the ratio between the number of Lagrangian particles and finite volume cells  $n_p/n_c$  and the radius of the concentration blob divided by the cell size:  $R_b/\delta$ . We found that for extremely large  $R_b/\delta$  values, our Euler-Lagrange model behaves like a single-phase model and thus loses crucial insights into the spatially varying fields of the nanoparticle volume fractions and the thermophysical properties, but provides good bulk results. On the other hand, for  $n_p/n_c \rightarrow \infty$  and  $R_b/\delta \rightarrow 0$ , our model behaves like the Euler-Euler model. This means that for a given choice of  $R_b$  and  $n_p$ , the proposed model works uniquely, unlike the single-phase and Euler-Euler models. The two parameters can be considered as optimization targets for our Euler-Lagrange model to capture the simulated phenomena more accurately.

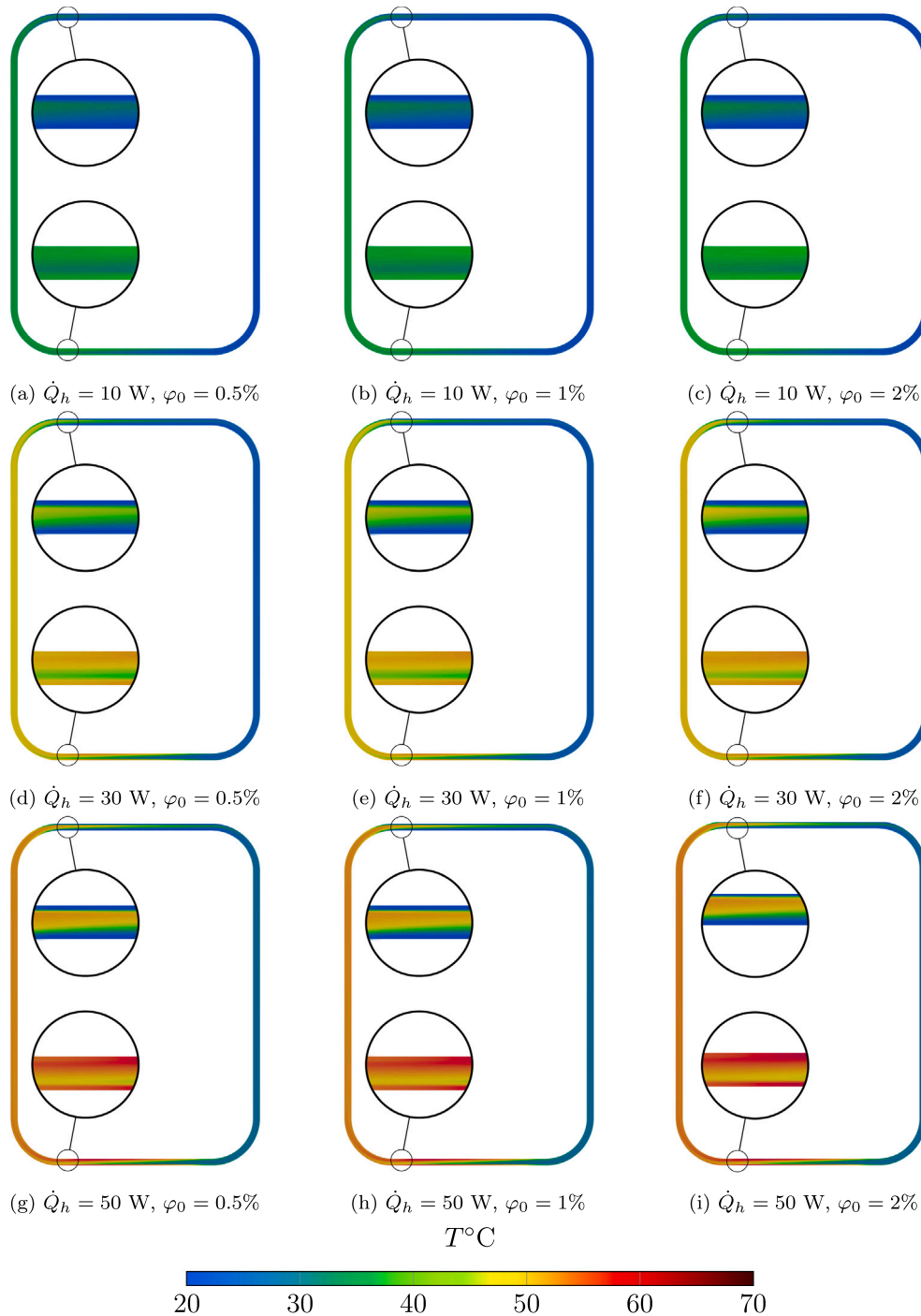


Fig. 16. NCL temperature fields, operating with nanofluid. The fluid flow circulates in the clockwise direction.

- The optimal value for the concentration blob radius, was found to be  $R_b/\delta = 20$ , for the Lagrangian particle to finite volume cell number ratio of  $n_p/n_c = 1$ . It means, that the simulated Lagrangian particle should have a volume fraction influence of 20 finite volume cells away from itself when the number of Lagrangian particles in our simulation is approximately the same as the number of cells, which is a reasonable assumption when simulating real heat exchangers.
- It was observed that, as expected, larger  $n_p/n_c$  ratios yield improved results. This observation led to the hypothesis that  $n_p/n_c$  can be treated as a discretization parameter, enabling the evaluation of the proposed method's order of convergence. To this end, a numerical uncertainty assessment was conducted, resulting in

a mean order of convergence of  $\bar{p} = 0.16$  and a mean numerical uncertainty of  $\overline{GCI} = 5.5\%$ .

- It was also found that the relative error of the nanoparticle volume fraction calculation is dependent on the local number of the Lagrangian particles, giving a larger error where the number of Lagrangian particles is lower. This can be a result of advection, thermophoresis, etc. The optimal value of  $R_b/\delta$  is therefore different in those regions, than in the bulk flow, giving larger errors.
- The results of the presented EL approach indeed follow the same trend as the experimental results and are in excellent agreement with the Euler–Euler and the single-phase implementations. The results for  $\Delta T$  show greater accuracy than the Euler–Euler and

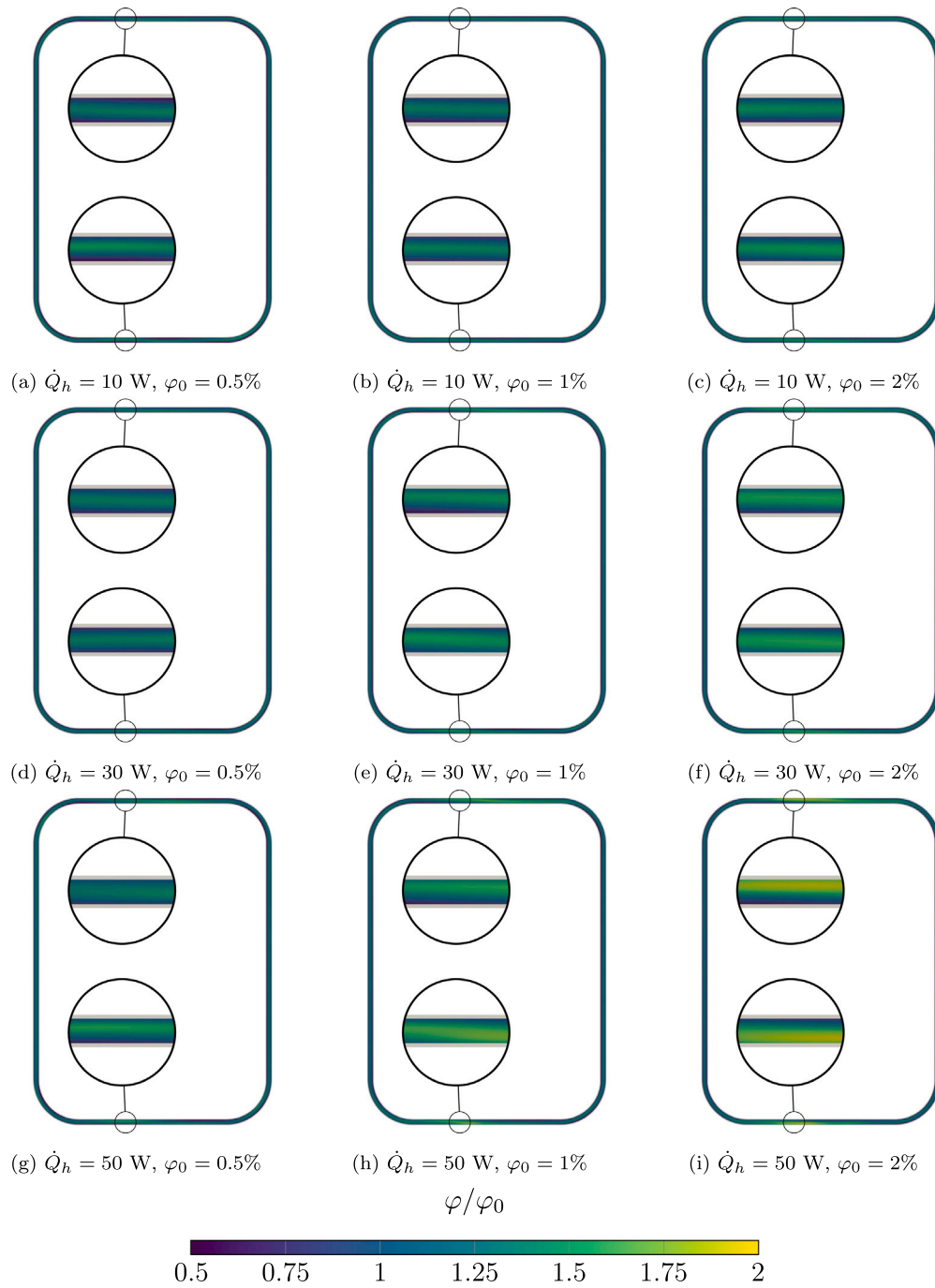


Fig. 17. NCL nanoparticle volume fraction fields, normalized to the bulk volume fraction. The presented fields are time-averaged over 500 s to 700 s.

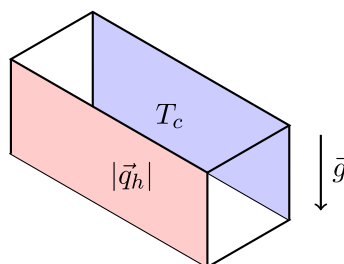


Fig. 18. The experimental geometry by Ho et al. [51]. The width and height of the enclosure measure 25 mm and the length measures 60 mm.

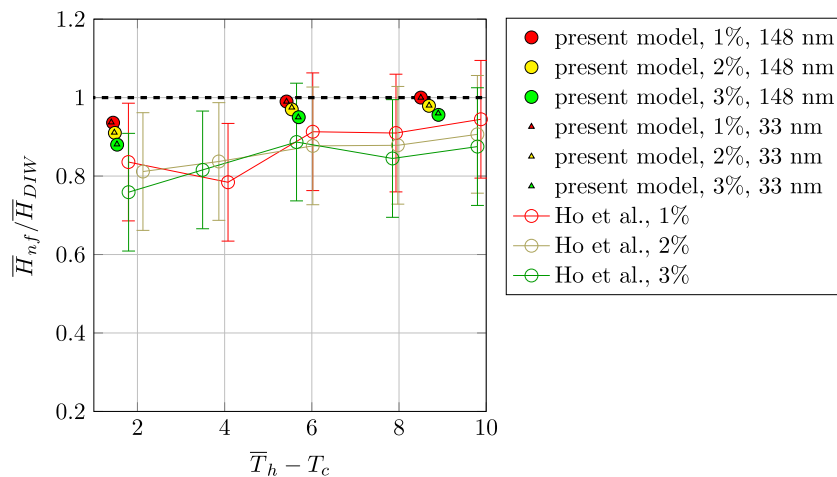


Fig. 19. Comparison of the experimental [51] and the present numerical model heat transfer coefficient ratio. The subscript  $nf$  corresponds to the nanofluid, while the  $DIW$  corresponds to the pure water simulation with the same setup.

the single-phase, while the  $T_{max}$  values show a very slight under-prediction. We attribute the discrepancy from the experimental results to the boundary conditions definition. We establish, that the interplay of multiple transport phenomena, that occur in nanofluid operated devices, are difficult to completely reproduce numerically within the framework of current modelling assumptions.

#### CRediT authorship contribution statement

**N. Vovk:** Writing – review & editing, Writing – original draft, Visualization, Validation, Software, Methodology, Investigation, Formal analysis, Data curation, Conceptualization. **B. Kamenik:** Writing – review & editing, Data curation, Conceptualization. **E. Begum Elcioglu:** Writing – review & editing, Supervision, Project administration, Funding acquisition, Formal analysis, Data curation. **E. Özyurt:** Writing – review & editing, Visualization, Methodology, Investigation, Formal analysis, Data curation. **Z.H. Karadeniz:** Writing – review & editing, Formal analysis. **A. Turgut:** Writing – review & editing, Formal analysis. **J. Ravnik:** Writing – review & editing, Writing – original draft, Supervision, Project administration, Funding acquisition, Formal analysis, Data curation, Conceptualization.

#### Declaration of competing interest

The authors declare that they have no known competing financial interests or personal relationships that could have appeared to influence the work reported in this paper.

#### Acknowledgements

The authors wish to thank the Slovenian Research and Innovation Agency for the financial support in the framework of the Programme P2-0196: Research in Power, Process and Environmental Engineering within the auspices of bilateral cooperation BI-TR/22-24-05. The authors also wish to thank the Scientific and Technological Research Council of Türkiye (TÜBİTAK) for the financial support in the framework of the Programme 2508 Bilateral Cooperation with Slovenian Research and Innovation Agency (grant no: 122N346), and Eskisehir Technical University Scientific Research Project (grant no: 21GAP072) for the financial support provided to purchase the circulating water bath used during viscosity measurements.

#### Data availability

Data will be made available on request.

#### References

- [1] Masataka Mochizuki, Randeep Singh, Thang Nguyen, Tien Nguyen, Heat pipe based passive emergency core cooling system for safe shutdown of nuclear power reactor, *Appl. Therm. Eng.* 73 (1) (2014) 699–706.
- [2] Sigit Santosa, M. Hadi Kusuma, Wegie Ruslan, Khusnul Khotimah, Giarno, Study of loop heat pipe prototype technology as a passive cooling system in nuclear reactors based on technology audit, in: THERMOFLUID XII: the 12th International Conference on Thermofluids 2021, Yogyakarta, Indonesia, 2024, 030001.
- [3] Zhiwei Wang, Zhongdi Duan, Yanping He, Chao Huang, Shiwen Liu, Hongxiang Xue, PIV-based experiments on reverse flow characteristics in an equal-height-difference passive heat removal system for ocean nuclear power plants, *Int. J. Heat Mass Transfer* 217 (2023) 124685.
- [4] S.U.S. Choi, Jeffrey Eastman, Enhancing thermal conductivity of fluids with nanoparticles, in: Proceedings of the ASME International Mechanical Engineering Congress and Exposition, vol. 66, 1995.
- [5] Nur Çobanoğlu, Ziya Haktan Karadeniz, Effect of nanofluid thermophysical properties on the performance prediction of single-phase natural circulation loops, *Energies* 13 (10) (2020) 2523.
- [6] S. Kakaç, A. Pramuanjaroenkij, Analysis of convective heat transfer enhancement by nanofluids: single-phase and two-phase treatments, *J. Eng. Phys. Thermophys.* 89 (3) (2016) 758–793.
- [7] Yacine Khetib, Hala M. Abo-Dief, Abdullah K. Alanazi, Hussein A. Saleem, S. Mohammad Sajadi, Mohsen Sharifpur, Simulation of alumina/water nanofluid flow in a micro-heat sink with wavy microchannels: impact of two-phase and single-phase nanofluid models, *Front. Energy Res.* 9 (2021) 760201.
- [8] M. Akbari, N. Galanis, A. Behzadmehr, Comparative analysis of single and two-phase models for CFD studies of nanofluid heat transfer, *Int. J. Therm. Sci.* 50 (8) (2011) 1343–1354.
- [9] M. Mahdavi, M. Sharifpur, J.P. Meyer, CFD modelling of heat transfer and pressure drops for nanofluids through vertical tubes in laminar flow by Lagrangian and Eulerian approaches, *Int. J. Heat Mass Transfer* 88 (2015) 803–813.
- [10] Omid Abouali, Goodarz Ahmadi, Computer simulations of natural convection of single phase nanofluids in simple enclosures: A critical review, *Appl. Therm. Eng.* 36 (2012) 1–13.
- [11] Majid Hejazian, Mostafa Keshavarz Moraveji, Alireza Beheshti, Comparative study of Euler and mixture models for turbulent flow of  $Al_2O_3$  nanofluid inside a horizontal tube, *Int. Commun. Heat Mass Transfer* 52 (2014) 152–158.
- [12] Jana Wedel, Mitja Štrakl, Matjaž Hriberšek, Paul Steinmann, Jure Ravnik, A novel particle–particle and particle–wall collision model for superellipsoidal particles, *Comput. Part. Mech.* 11 (1) (2024) 211–234.
- [13] Jana Wedel, Matjaž Hriberšek, Jure Ravnik, Paul Steinmann, A novel pseudo-rigid body approach to the non-linear dynamics of soft micro-particles in dilute viscous flow, *J. Comput. Phys.* 519 (2024) 113377.
- [14] Mohammad Farazm, George Haller, The Maxey–Riley equation: Existence, uniqueness and regularity of solutions, *Nonlinear Anal. Real World Appl.* 22 (2015) 98–106.
- [15] Amy Li, Goodarz Ahmadi, Dispersion and deposition of spherical particles from point sources in a turbulent channel flow, *Aerosol Sci. Technol.* 16 (4) (1992) 209–226.
- [16] Yurong He, Yubin Men, Yunhua Zhao, Huilin Lu, Yulong Ding, Numerical investigation into the convective heat transfer of  $TiO_2$  nanofluids flowing through a straight tube under the laminar flow conditions, *Appl. Therm. Eng.* 29 (10) (2009) 1965–1972.

- [17] Saman Rashidi, Masoud Bovand, Javad Abolfazli Esfahani, Goodarz Ahmadi, Discrete particle model for convective Al<sub>2</sub>O<sub>3</sub>-water nanofluid around a triangular obstacle, *Appl. Therm. Eng.* 100 (2016) 39–54.
- [18] Mahla Maskaniyan, Saman Rashidi, Javad Abolfazli Esfahani, A two-way couple of Eulerian-Lagrangian model for particle transport with different sizes in an obstructed channel, *Powder Technol.* 312 (2017) 260–269.
- [19] Omar Z. Sharaf, Ashraf N. Al-Khateeb, Dimitrios C. Kyritsis, Eiyad Abu-Nada, Numerical investigation of nanofluid particle migration and convective heat transfer in microchannels using an Eulerian-Lagrangian approach, *J. Fluid Mech.* 878 (2019) 62–97.
- [20] Mehdi Bahiraei, A numerical study of heat transfer characteristics of CuO-water nanofluid by Euler-Lagrange approach, *J. Therm. Anal. Calorim.* 123 (2) (2016) 1591–1599.
- [21] Jonas Burggraf, Peter Farber, Kavien Raaj Karpaiya, Peer Ueberholz, Numerical investigation of laminar flow heat transfer of TiO<sub>2</sub>-water nanofluid in a heated pipe, *Heat Transf. Eng.* 42 (19–20) (2021) 1635–1647.
- [22] Zhaoyin Yin, Fubin Bao, Chengxu Tu, Yicong Hua, Rui Tian, Numerical and experimental studies of heat and flow characteristics in a laminar pipe flow of nanofluid, *J. Exp. Nanosci.* 13 (1) (2018) 82–94.
- [23] R. Deepak Selvakumar, S. Dhinakaran, Heat transfer and particle migration in nanofluid flow around a circular bluff body using a two-way coupled Eulerian-Lagrangian approach, *Int. J. Heat Mass Transfer* 115 (2017) 282–293.
- [24] Ahmed S. Habeeb, Abdulhassan A. Karamallah, Sattar Aljabair, Review of computational multi-phase approaches of nano-fluids filled systems, *Therm. Sci. Eng. Prog.* 28 (2022) 101175.
- [25] Bijan Darbari, Mohammad Bagher Ayani, Heat transfer and deposition analysis of CuO-water nanofluid inside a baffled channel: Two-phase Eulerian-Lagrangian method, *J. the Taiwan Inst. Chem. Eng.* 148 (2023) 104827.
- [26] Kotaro Fujimoto, Aima Shibata, Shuichi Torii, An experimental and numerical study of turbulent heat transfer enhancement for graphene nanofluids produced by pulsed discharge, *Int. J. Thermofluids* 16 (2022) 100219.
- [27] M. Mahdavi, M. Sharifpur, J.P. Meyer, Discrete modelling of nanoparticles in mixed convection flows, *Powder Technol.* 338 (2018) 243–252.
- [28] Mostafa Mahdavi, Mohsen Sharifpur, Mohammad H. Ahmadi, Josua P. Meyer, Aggregation study of Brownian nanoparticles in convective phenomena, *J. Therm. Anal. Calorim.* 135 (1) (2019) 111–121.
- [29] Ismail Celik, Ghia Urmila, Roache Patrick J., Freitas Christopher J., Procedure for estimation and reporting of uncertainty due to discretization in CFD applications, *J. Fluids Eng.* 130 (7) (2008) 078001.
- [30] Abdul Hai Alami, Mohamad Ramadan, Muhammad Tawalbeh, Salah Haridy, Shamma Al Abdulla, Haya Aljaghoub, Mohamad Ayoub, Adnan Alashkar, Mohammad Ali Abdelkareem, Abdul Ghani Olabi, A critical insight on nanofluids for heat transfer enhancement, *Sci. Rep.* 13 (1) (2023) 15303.
- [31] M.H. Buschmann, R. Azizian, T. Kempe, J.E. Juliá, R. Martínez-Cuenca, B. Sundén, Z. Wu, A. Seppälä, T. Ala-Nissila, Correct interpretation of nanofluid convective heat transfer, *Int. J. Therm. Sci.* 129 (2018) 504–531.
- [32] B. Kamenik, E. Begum Elcioglu, A. Turgut, R. Mondragón, L. Hernandez Lopez, J.P. Vallejo, L. Lugo, M.H. Buschmann, J. Ravník, Numerical analysis of performance uncertainty of heat exchangers operated with nanofluids, *Int. J. Thermofluids* 14 (2022) 100144.
- [33] J.S. Marshall, K. Sala, Comparison of methods for computing the concentration field of a particulate flow, *Int. J. Multiph. Flow* 56 (2013) 4–14.
- [34] H.G. Weller, G. Tabor, H. Jasak, C. Fureby, A tensorial approach to computational continuum mechanics using object-oriented techniques, *Comput. Phys.* 12 (6) (1998) 620–631.
- [35] Utkarsh Ayachit, *The ParaView Guide: Updated for ParaView Version 4.3*, Kitware Inc, Clifton Park, NY, 2015, full color version edition.
- [36] M. Chandrasekar, S. Suresh, A. Chandra Bose, Experimental investigations and theoretical determination of thermal conductivity and viscosity of Al<sub>2</sub>O<sub>3</sub>-water nanofluid, *Exp. Therm. Fluid Sci.* 34 (2) (2010) 210–216.
- [37] Bhavin Mehta, Dattatraya Subhedar, Synthesis and characterization of  $\gamma$ -Al<sub>2</sub>O<sub>3</sub>-water nanofluid with and without surfactant, *Mater. Today: Proc.* 62 (2022) 418–425.
- [38] Thaklaew Yiamsawas, Ahmet Selim Dalkilic, Omid Mahian, Somchai Wongwises, Measurement and correlation of the viscosity of water-based Al<sub>2</sub>O<sub>3</sub> and TiO<sub>2</sub> nanofluids in high temperatures and comparisons with literature reports, *J. Dispers. Sci. Technol.* 34 (12) (2013) 1697–1703.
- [39] E. Begum Elcioglu, *Experimental and Theoretical Investigations on Alumina-Water Nanofluid Viscosity with Statistical Analysis* (MSc thesis), Middle East Technical University, Ankara, Turkiye, 2013.
- [40] A. Einstein, Eine neue Bestimmung der Moleküldimensionen, *Ann. Phys., Lpz.* 324 (2) (1906) 289–306.
- [41] Alpaslan Turgut, *Investigation of Thermophysical Properties of Nanofluids* (Ph.D. thesis), Dokuz Eylul Universitesi, Izmir, Turkiye, 2010.
- [42] Hidetoshi Masuda, Akira Ebata, Kazunari Teramae, Nobuo Hishinuma, Alteration of thermal conductivity and viscosity of liquid by dispersing ultra-fine particles. Dispersion of Al<sub>2</sub>O<sub>3</sub>, SiO<sub>2</sub> and TiO<sub>2</sub> ultra-fine particles, *Netsu Bussei* 7 (4) (1993) 227–233.
- [43] Sarit Kumar Das, Nandy Putra, Peter Thiesen, Wilfried Roetzel, Temperature dependence of thermal conductivity enhancement for nanofluids, *J. Heat Transf.* 125 (4) (2003) 567–574.
- [44] X. Zhang, H. Gu, M. Fujii, Experimental study on the effective thermal conductivity and thermal diffusivity of nanofluids, *Int. J. Thermophys.* 27 (2) (2006) 569–580.
- [45] S.M.S. Murshed, K.C. Leong, C. Yang, Investigations of thermal conductivity and viscosity of nanofluids, *Int. J. Therm. Sci.* 47 (5) (2008) 560–568.
- [46] James Clerk Maxwell, *A Treatise on Electricity and Magnetism*, vol. 2, Cambridge University Press, Cambridge, 2010.
- [47] J. Buongiorno, Convective transport in nanofluids, *J. Heat Transf.* 128 (3) (2006) 240–250.
- [48] G.S. McNab, A. Meisen, Thermophoresis in liquids, *J. Colloid Interface Sci.* 44 (2) (1973) 339–346.
- [49] Habib Aminfar, Mohammad Reza Haghgo, Brownian motion and thermophoresis effects on natural convection of alumina-water nanofluid, *Proc. Inst. Mech. Eng. C* 227 (1) (2013) 100–110.
- [50] Blaž Kamenik, Nejc Vovk, Elif Begum Elcioglu, Firat Sezgin, Erdem Ozyurt, Ziya Haktan Karadeniz, Alpaslan Turgut, Jure Ravník, Euler-Euler numerical model for transport phenomena modeling in a natural circulation loop operated by nanofluids, *Int. J. Thermophys.* 46 (3) (2025) 40.
- [51] C.J. Ho, W.K. Liu, Y.S. Chang, C.C. Lin, Natural convection heat transfer of alumina-water nanofluid in vertical square enclosures: An experimental study, *Int. J. Therm. Sci.* 49 (8) (2010) 1345–1353.